Molecular dynamics simulation of penetrants transport in composite poly (4-methyl-2-pentyne) and nanoparticles of different types

Quan Yang

Dissertation submitted to the faculty of the Virginia Polytechnic Institute and State University in partial fulfillment of the requirements for the degree of

Doctor of Philosophy
In
Chemical Engineering

Luke E. Achenie, Chair
David F. Cox
Richey M. Davis
Peter B. Rim

Nov. 15, 2013
Blacksburg, Virginia

Keywords: Molecular dynamics simulation; composite PMP and silica nanoparticle composite; cristobalite silica; faujasite silica

Molecular dynamics simulation of penetrants transport in composite poly (4-methyl-2-pentyne) and nanoparticles of different types

Quan Yang

Abstract

Membranes made of composite polymer material are widely employed to separate gas mixtures in industrial processes. These membranes have better performance than membranes consisting of polymer alone. To understand the mechanism and therefore aid membrane design it is essential to explore the penetrant transport in the complex composites from the molecular level, but few researchers have done such research to our knowledge. Herein the penetrant transport in the composite Poly (4-methyl-2-pentyne) (PMP) and silica nanoparticle has been explored with molecular dynamics (MD) simulations. The structure of the PMP and amorphous silica nanoparticle composite was modeled and subsequently the variation of the cavity size distribution was established in the presence of nanoparticles. The diffusivity of different penetrants, including H_2, O_2, Ar, CH_4 and n-C_4H_{10} was determined through a least squares fit of the displacement at different times in the Fickian diffusive regime. The solubility coefficients and the permeability of different penetrants in PMP and the composite were calculated and the distribution of potential difference due to the penetrant insertion was analyzed in detail to find the reason for the higher solubility in the composite than in pure PMP. Silica has different crystalline forms. In faujasite silica, there are pores that are large enough to allow penetrants to pass through, while in cristobalite silica, the Si and O atoms are densely packed; therefore there are virtually no pores through which penetrants can pass. The transport properties of penetrants in the composite (consisting of PMP and nanoparticles) of the

two types of silica are therefore different. The molecular dynamics method was employed in the research to explore the transport of different penetrants in the composites of PMP and nanoparticles of two forms of silica, namely the cristobalite form and the faujasite form. The structures of the PMP and cristobalite silica nanoparticle composite (PMPC) on one hand, and the PMP and faujasite silica nanoparticle composite (PMPF) on the other hand were established and relaxed. With the relaxed structure, the cavity size change due to the insertion of both types of nanoparticle was analyzed. The diffusivity of different penetrants was determined through a least square fit of the mean square displacement at different times in the Fickian diffusive regime. The solubility coefficients and the permeability of different penetrants in PMPC and PMPF were calculated and compared. The parameters of 'Ti' in the Lennard-Jones potential equation were estimated; MD simulation of penetrants transport in composite poly (4-methyl-2-pentyne) and TiO_2 nanoparticles were done. Finally the simulation results were compared with composite poly (4-methyl-2-pentyne) and silica nanoparticles.

Acknowledgements

I would like to thank my advisor Professor Achenie, who guides me through the whole process. I also acknowledge all professors of my committee. You spend your precious time to read the dissertation and attend the committee meeting. Thank you.

I would also show my acknowledgement to my colleagues, like Christopher Christie. They are nice and tend to give people help.

Finally I will thank my parents and all my good friends. It is because of you that I gather enough motivation to pursue my Ph.D. degree. Now I have got very good results in my research. Thank you all.

Table of contents

List of tables

List of figures

Chapter 1

Introduction

1.1 Significance of the project

In industry, the separation of methane from higher hydrocarbons, organic monomers from nitrogen and others are important separation processes. In the production of natural gas, raw gas must always be treated to separate butane and higher hydrocarbons from the methane to bring the heating value and the dew point to pipeline specification, and to recover the valuable higher hydrocarbons as chemical feedstock. Similarly, approximately 1% of the 30 billion lb/year of monomer used in polyethylene and polypropylene production is lost in the nitrogen vent streams from resin purge operation. Recovery of these monomers would save US producers about $100 million/year [1].

In these processes, instead of membranes consisting of polymer solely, membranes made of composite material [2] are used due to their better performance than membranes. For example, the PMP and silica nanoparticle composite is used to separate C_4H_{10} (n-butane) from mixtures of C_4H_{10} and CH_4, H_2, etc.

A large amount of experimental research has been done to explore the penetrant transport in the composite [3-12]. However, to understand the mechanism and therefore aid membrane design, it is essential to explore the properties of complex composites from the molecular level [13-22]. Molecular dynamics (MD) simulation is an excellent method that is extensively employed to explore the transport properties of penetrants in organic polymers and inorganic

materials from the molecular level [23-32]. Most researchers do MD simulation to simulate penetrants transport in different pure materials. Boshoff et al. [33] simulated the diffusion of helium in polypropylene (PP). Charati and Stern [34] explored the penetrant transport in different silicone polymers, including poly (dimethylsiloxane) (PDMS), poly (propylmethylsiloxane) (PPMS), poly ((trifluoropropyl)methylsiloxane) (PTFPMS), and poly (phenylmethylsiloxane) (PPhMS) through molecular dynamics simulation. Tamai et al. [35] estimated the diffusivity of methane, water, and ethanol in polyethylene (PE) and PDMS via MD simulation. Müller-Plathe et al. [36] used MD simulation to research the diffusion of oxygen and helium in amorphous polyisobutylene (PIB). Gee and Royd [37] simulated the diffusion of methane in polybutadiene (PBD). Karlsson, et al. [38] explored the oxygen diffusion in dry and water-containing poly(vinyl alcohol) (PVA) with MD simulation. Pavel and Shanks [39] did molecular dynamics simulation of diffusion of O_2 and CO_2 in blends of amorphous poly(ethylene terephthalate) and related polyesters. Amrani and Kolb [40] did molecular dynamics simulations in zeolites. All of these studies are on penetrants transport in polymer, blends, or ceramics. However, to our knowledge, few researchers have explored the transport property of penetrants in composites using MD simulation. This is the main motivation for this dissertation. Smith, et. al [2] only simulated the properties of an imaginary model composite system. It is imaginary because the author set the size of the balls consisting of the polymer chains and the interactions, like VDW, electrostatic interaction according to his wish, not real polymer.

1.2 Classification of membrane materials [41, 42]

Membranes have been extensively employed in micro-filtration, ultra-filtration, reverse-osmosis and gas separation. In gas separation, the factors that determine the efficiency of the penetrant transport process are the selectivity and permeability of the membrane material. As a

result, based on the permeability (or flux density) and selectivity of the membranes, they can be classified into two different categories: porous and non-porous.

A porous material consists of rigid, highly voided structure with randomly distributed pores; the separation of penetrants with this type of membrane depends on the molecular size of membrane polymer, cavity size and cavity size distribution. A porous membrane is like a conventional filter when membranes have pore diameters between those of the penetrant molecules to be separated. In such case only those molecules that differ considerably in size can be separated effectively with porous membranes. For Knudsen flow the selectivity can be estimated according to the square root of the ratio of the molecular weights. So either molecule size or weight can determine selectivity. When surface diffusion mechanism applies, the molecule size takes effect, while when Knudsen diffusion happens, the molecule weight is the most important factor that determines selectivity.

Porous membranes have high flux but low selectivity in the separation process. They are characterized with the average pore diameter, the membrane porosity (the fraction of the total membrane volume that is porous) and the tortuosity of the membrane. In the research, I am interested in membranes that can separate penetrants that do not differ considerably in size. Therefore porous membranes cannot satisfy our requirement.

In contrast, non-porous or dense membranes have high selectivity in the separation of gas mixtures. However, the flux is low. Unlike porous membranes, non-porous membranes are capable of separating penetrants of similar sizes if their solubility in the membrane differs significantly. In our research, the polymer PMP belongs to this category.

1.3 Mechanisms of penetrant transport

Various mechanisms for penetrant transport across different materials (polymer, ceramics, composite, etc.) have been proposed according to the properties of both the penetrants and the materials, including Knudsen diffusion, molecular sieve (surface diffusion) and solution diffusion mechanisms.

1.3.1 Mechanisms through porous materials

When penetrants are transported through a porous membrane, different mechanisms may exist [42-44].

Mechanism (a): The transport of penetrants through porous membranes includes Knudsen diffusion and Poiseuille flow. The ratio of Knudsen to Poiseuille flow is determined through the ratio between the pore radius and the mean free path of molecules which is computed as:

$$\lambda = \frac{3\eta}{2p} \cdot \frac{\sqrt{\pi RT}}{2M} \tag{1}$$

where η is the viscosity of the penetrants, R the universal gas constant, T the temperature, M the molecular weight and p the pressure.

For Knudsen flow, according to the equation present above, the selectivity can be estimated according to the square root of the ratio of the molecular weights. Knudsen separation is observed for membranes with pore sizes smaller than 50nm [44].

Mechanism (b): When membranes have pore diameters between those of the penetrant molecules to be separated, the membrane would function as a molecular sieve and the surface diffusion mechanism is involved in the process. In such a case, only the smaller molecules can permeate and high selectivity can be achieved, especially if the pore sizes in the membranes are smaller than about 0.5nm [45].

Mechanism (c): Some components of a mixture can condense in the pores of the membrane materials, with the exclusion of others. The component then permeates through the pore and is separated from the mixture.

Mechanism (d): Certain components of a mixture are adsorbed onto the pore surface and then the adsorbed molecule is transported across the pore with the surface diffusion mechanism involved.

Separation process governed by Knudsen mechanism generally has very low selectivity, while mechanism (b) corresponds to high selectivity and permeability for smaller component of a mixture [41, 42]. Mechanism (c) requires the pore size of membrane materials to be in the meso-porous size range (diameter>30 angstrom), so that condensation of the component can take place. High selectivity can be achieved but the extent of removal of the condensable component from mixture is limited by the condensation partial pressure of that component. Mechanism (d) gives the most flexible choice for practical separation of mixtures, because the selectivity is determined by both adsorption and diffusion of the absorbed molecules.

1.3.2 Mechanism through non-porous membranes

The mechanism for penetrants transport through dense non-porous material is different from that of porous materials. The solution-diffusion mechanism describes the penetrants transport through dense polymeric materials. In the solution-diffusion mechanism, the penetrants dissolve in the membrane material and then diffuse through the material along a concentration gradient.

The mechanism consists of three steps: (1) the absorption or adsorption of penetrants at the upstream boundary; (2) activated diffusion (solubility) through the membrane; and (3) desorption or evaporation of the transported penetrants on the other side of the membrane

materials.

As a result, the driving force of the solution-diffusion process includes the difference in the thermodynamic activities at the upstream and downstream sides of the membrane material and the interaction between membrane molecules and the penetrant molecules.

The permeability is the product of the solubility and diffusion coefficient. However, the formulation of these coefficients is difficult. The penetrant transport differs much in the rubbery and glassy states in polymers, i.e. at temperatures above and below the glass transition temperature of the polymers. Plasticization due to the penetrants also makes the formulation even more complicated. Therefore though there are transport models proposed in the literature, they are phenomenological in nature and contain adjustable parameters to be determined experimentally [47-50].

1.4 Models explaining penetrant transport

The models developed to explain penetrant transport are to be presented.

1.4.1 Microscopic models

Because different mechanisms are involved when penetrants are transported in different materials, a number of models have been proposed to describe the process. Free volume models [51-54] are proposed for transport in rubbery polymers. Fujita [55] proposed a model to describe a strong concentration dependence of organic vapors in rubbery polymers. Vrentas and Duda [56] proposed free volume model of diffusion, which provided an expression for the mutual diffusion coefficient for solvent/polymer systems as a function of solvent concentration. Ganesh et al. [57] have improved the free volume model to predict permeability in polymers. Empirical correlations between permeability or diffusivity and free volume of polymers, or of penetrant/polymer systems have also been proposed [58-61].

The dual-mode sorption model was proposed by Paul and Koros [62, 63] and by Petropoulos [64] to do phenomenological description of penetrant transport in glassy polymer [65, 66, 64]. The model satisfactorily gives the relationship between solubility, diffusivity, permeability, and the concentration of penetrants [67].

These phenomenological models are functionally limited because they are not predictive and the model parameters are not directly related to the chemical structure of polymers.

All these microscopic models are limited to certain systems and none of there is applicable to our composite systems.

1.4.2 Molecular models

Due to the limitation of microscopic models, molecular theories were finally employed to explain the mechanism of penetrant transport. Brandt [68] and Dibenedetto [69] analyzed a diffusion process in terms of specific postulated motions of polymer chains relative to each other and motion of penetrant molecules.

Brandt [68] proposed a model where a penetrant molecule pushes a "polymer?" chain and jumps into a new position as it moves through the polymer matrix. In Dibenedetto's [69] model, the polymer segments can be in a normal or activated state. In the activated state the polymer chain accepts a diffusing molecule, allows it to diffuse, and then returns to normal state after the jump. The model proposed by Pace and Datyner [70-72] considers the structure of polymers.

Based on these concepts, in the last few years computer software has been developed to simulate the penetrant transport in polymers. Molecular dynamics is increasingly used as a powerful tool for exploring such transport phenomena. These simulation methods explore the transport at the molecular level and give a link between chain architecture, force field and

penetrant transport that can be used in the design and optimization of separation membranes [73, 74].

Researchers have successfully carried out molecular dynamics simulation for polyethylene, rubber networks, atactic polypropylene, polyisobutylene and poly-(dimethy(siloxane)), polycarbonate and polyamide, etc. [75-84]. These simulations have results that are in agreement with experimental values; however, few researchers have done such wok to explore the composite systems as I have done in the research.

1.5 MD simulation

The knowledge of MD simulation is to be introduced.

1.5.1 MD simulation algorithm

One performs Molecular dynamics (MD) simulations in order to understand the properties of systems (assemblies) of particles (atoms, molecules or units composed of a certain number of atoms) through simulating their structure and the interactions among them. MD simulations complement wet lab experiments, and can provide us new knowledge that cannot be obtained with other methods.

MD simulations act as a bridge between the length and time scales of molecular level phenomena and macroscopic phenomena as usually observed in a laboratory. To begin the simulation a guess at the interactions between molecules is given. The simulation results are then used to estimate bulk properties. The estimates can be made as accurately as desired, subject to the availability of computing resources and the quality of the MD algorithm. Important insights into bulk measurements can be revealed. An example is the connection between the diffusion coefficient and velocity autocorrelation function (the former is easy to measure experimentally, while the latter is much harder). MD simulations behave as a bridge

between theory and experiment in another sense. People can test a theory by conducting a simulation using the same model and can test the model through comparing the computed results with experimental results. People can also perform simulations on the computer that are difficult or impossible in the laboratory (e. g., working at extremes of temperature or pressure).

Molecular dynamics is a computer simulation of physical movements of particles (atoms, molecules or units). The atoms and molecules are observed to interact with each other for a given time, resulting in a view of the motion of the atoms. In most MD implementations, the trajectories of molecules and atoms are determined by numerically solving the Newton's equations of motion for a system of interacting particles. Forces between the particles and potential energy are defined by molecular mechanics force fields. The method was originally conceived within theoretical physics in the late 1950s [85] and early 1960s [86], but is applied today mostly in materials science and molecular modeling in general.

Because molecular systems consist of a vast number of particles, it is impossible to find the properties of such complex systems analytically; MD simulation circumvents this problem by using numerical methods.

The results of molecular dynamics simulations can be used to determine thermodynamic properties of the system based on the ergodic hypothesis: the statistical ensemble averages equal the time averages of the system. MD has also been termed “Laplace's vision of Newtonian mechanics” of predicting the future by simulating nature's forces [87, 88] and allowing insight into molecular motion on an atomic scale.

Figure 1.1 is a description of the molecular dynamics simulation algorithm. The simulation iteratively proceeds through calculating forces and solving the equations of motion according to the accelerations obtained from the new forces at new steps. In practice, almost all MD codes use different versions of the algorithm [89] (e.g. the two-step algorithm, predictor and corrector) when solving the equations of motion and several-step algorithm for temperature

and pressure control, analysis, and output.

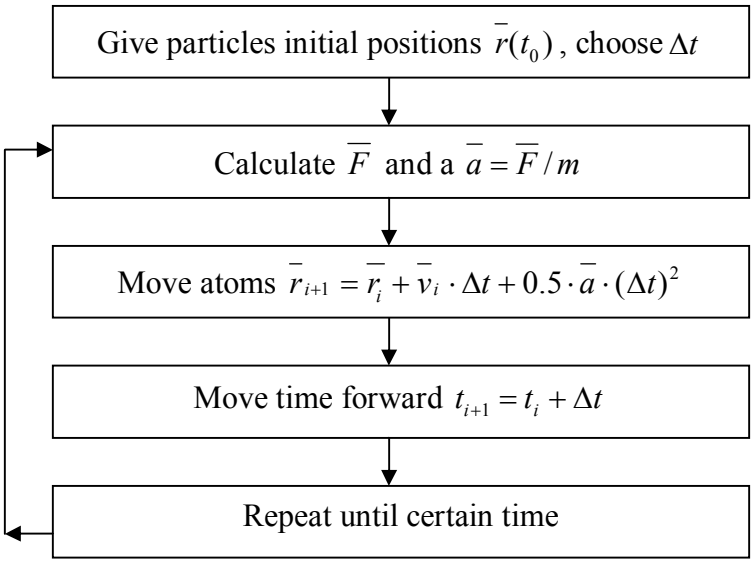

Figure 1.1 Flow sheet to show the molecular dynamics simulation algorithm

It is needed to do integration in the MD algorithm in Figure 1.1. In DLPOLY software, the Verlet algorithm is employed to do the integration of the Newton equations. There are two versions of the Verlet algorithm, namely the leapfrog Verlet (LF) algorithm and the velocity Verlet (VV) algorithm.

The Verlet Leapfrog algorithm requires values of position and force at time *t* while the velocities are half a time step (Δt) behind or ahead time *t*. The first step is to calculate the velocities at time $t + 0.5\Delta t$ though integration of force according to the following equation:

$$\underline{v}(t + 0.5\Delta t) = \underline{v}(t - 0.5\Delta t) + \Delta t \frac{\underline{f}(t)}{m} \tag{2}$$

The position is then computed using the velocities at time $t + 0.5\Delta t$:

$$\underline{r}(t + \Delta t) = \underline{r}(t) + \Delta t \cdot \underline{v}(t + 0.5\Delta t) \tag{3}$$

Molecular dynamics simulations normally require properties that depend on position and velocity at the same time (such as the sum of potential and kinetic energy). So the velocities at time *t* should be obtained. The velocities at time *t* are evaluated according to the equation:

$$\underline{v}(t) = \frac{\underline{v}(t + 0.5\Delta t) + \underline{v}(t - 0.5\Delta t)}{2} \tag{4}$$

Different from the leapfrog Verlet algorithm, the velocity Verlet algorithm assumes that positions, velocities, and forces are known at each full time step.

The algorithm proceeds in two stages as follows. In the first stage a half step velocity is calculated:

$$\underline{v}(t + 0.5\Delta t) = \underline{v}(t) + \Delta t \frac{\underline{f}(t)}{2m} \tag{5}$$

and then the full time step position is obtained:

$$\underline{r}(t + \Delta t) = \underline{r}(t) + \Delta t \cdot \underline{v}(t + 0.5\Delta t) \tag{6}$$

In the second stage, using the new positions, the next update of the forces $\underline{f}(t + \Delta t)$ is obtained, from which the full step velocity is calculated using the equation:

$$\underline{v}(t + \Delta t) = \underline{v}(t + 0.5\Delta t) + \Delta t \frac{\underline{f}(t + \Delta t)}{2m} \tag{7}$$

Thus at the end of the two stages all the values of the positions, forces and velocities are obtained.

1.5.2 Force field

The interactions between particles of the systems have two types: intermolecular and intramolecular interaction. The potential functions are employed to estimate the interactions. Figure 1.2 shows the geometry of a chain molecule and illustrate the definition of interatomic distance r_{ab}, bend angle θ_{bcd}, and torsion angle ϕ_{abcd}.

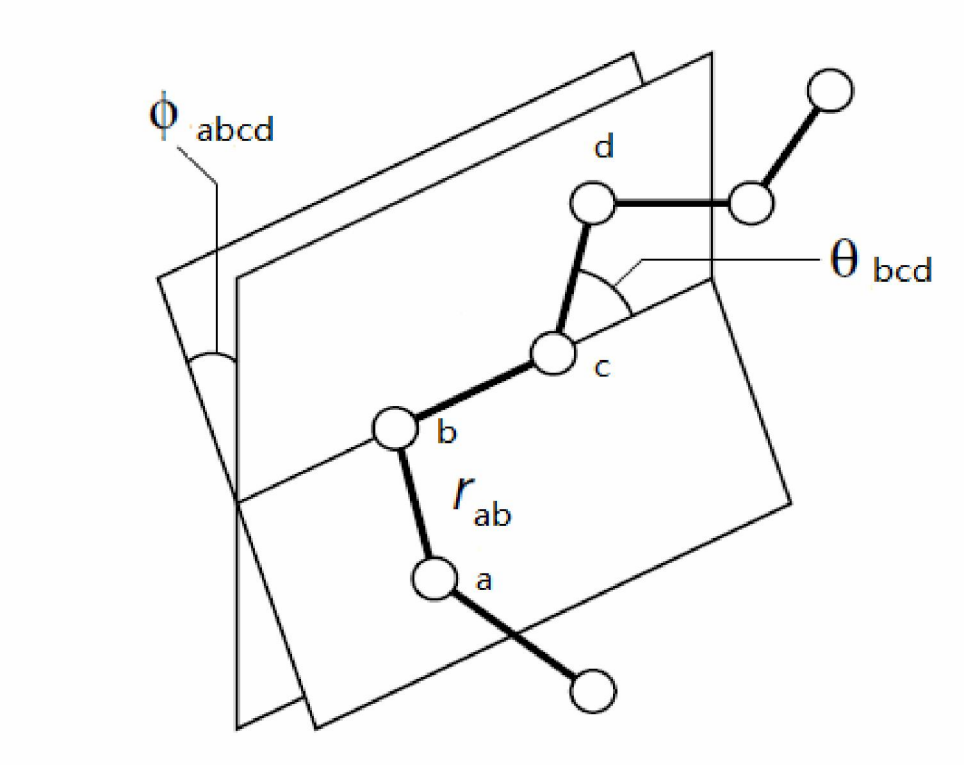

Figure 1.2. Geometry of a chain molecule, illustrating the definition of interatomic distance r_{ab}, bend angle θ_{bcd}, and torsion angle ϕ_{abcd}.

The considered intramolecular include the following types:

(I) Bond interaction (Potentials)

The bond potentials describe explicit chemical bonds between specified atoms. They are all functions of the interatomic distance r_{ab}. The functions have harmonic form, Morse form, 12-6 form [89] etc.

1. Harmonic form, which is the most frequently used:

$$U(r_{ab}) = \frac{1}{2}k(r_{ab} - r_0)^2 \tag{8}$$

where r_0 is the equilibrium interatomic distance and *k* is bond force constant.

2. Morse form:

$$U(r_{ab}) = E_0\{[1 - \exp(-k(r_{ab} - r_0))]^2 - 1\} \tag{9}$$

where r_0 is the equilibrium interatomic distance, *k* is bond force constant and r_{ab} represents the interatomic distance.

3. 12-6 form:

$$U(r_{ab}) = (\frac{A}{r_{ab}^{12}}) - (\frac{B}{r_{ab}^{6}}) \tag{10}$$

4. Quartic form:

$$U(r_{ab}) = \frac{1}{2}k(r_{ab} - r_0)^2 + \frac{1}{3}k'(r_{ab} - r_0)^3 + \frac{1}{4}k''(r_{ab} - r_0)^4 \tag{11}$$

5. Buckingham form:

$$U(r_{ab}) = A\exp(-\frac{r_{ab}}{\rho}) - \frac{C}{r_{ab}^6} \tag{12}$$

where the first term is the potential due to repulsive force while the second term represents the potential due to attractive force.

(II) Valence Angle Potentials

The valence angle potentials describe the bond bending terms between the specified atoms. The valence angle potentials have harmonic form, quartic form, harmonic cosine form and cosine form, etc. The most frequently employed form is also the harmonic form of the potential.

1. Harmonic potential:

$$U(\theta_{bcd}) = \frac{1}{2}k(\theta_{bcd} - \theta_0)^2 \tag{13}$$

where θ_0 is the equilibrium angel and *k* is angel constant.

2. Quartic form:

$$U(\theta_{bcd}) = \frac{1}{2}k(\theta_{bcd} - \theta_0)^2 + \frac{1}{3}k'(\theta_{bcd} - \theta_0)^3 + \frac{1}{4}k''(\theta_{bcd} - \theta_0)^4 \tag{14}$$

3. Harmonic cosine:

$$U(\theta_{bcd}) = \frac{1}{2}k(\cos\theta_{bcd} - \cos\theta_0)^2 \tag{15}$$

4. Cosine:

$$U(\theta_{bcd}) = A[1 + \cos(m\theta_{bcd} - \delta)] \tag{16}$$

where *A*, *m* and δ are constants which have different values corresponding to different types of bond angles.

(III) Dihedral Angle Potentials

The dihedral angle potentials describe the interaction arising from torsional forces in molecules. They are sometimes referred to as torsion potentials. They require the specification of four atomic positions. The most frequently used potentials include harmonic potential, harmonic cosine potential, cosine potential, triple cosine potential and OPLS angle potential.

1. Harmonic potential:

$$U(\theta_{abcd}) = \frac{1}{2}k(\theta_{abcd} - \theta_0)^2 \tag{17}$$

where θ_{abcd} is the dihedral angel to be computed, θ_0 is the equilibrium dihedral angel and *k* is the dihedral angel potential constant.

2. Harmonic cosine potential:

$$U(\theta_{abcd}) = \frac{1}{2}k(\cos\theta_{abcd} - \cos\theta_0)^2 \tag{18}$$

3. Cosine potential:

$$U(\phi_{abcd}) = A[1 + \cos(m\phi_{abcd} - \delta)] \tag{19}$$

where A, m, δ are constants relevant to the types of particles that compose the dihedral angle.

4. Triple cosine potential:

$$U(\phi_{abcd}) = \frac{1}{2}[A_1(1 + \cos\phi_{abcd}) + A_2(1 - \cos 2\phi_{abcd}) + A_3(1 + \cos 3\phi_{abcd})] \tag{20}$$

where A_1, A_2 and A_3 are constants relevant to the types of particles that compose the dihedral angle.

5. OPLS angle potential:

$$U(\phi_{abcd}) = A_0 + \frac{1}{2}[A_1(1 + \cos\phi_{abcd}) + A_2(1 - \cos 2\phi_{abcd}) + A_3(1 + \cos 3\phi_{abcd})] \tag{21}$$

Where A_0, A_1, A_2 and A_3 are constants relevant to the types of particles that compose the dihedral angle.

The considered intermolecular interactions include the following types:

(I) VDW potentials

The most widely used functions used to calculate VDW potentials include the following types:

Lennard-Jones potential:

$$U(r_{ab}) = 4\varepsilon[(\frac{\sigma}{r_{ab}})^{12} - (\frac{\sigma}{r_{ab}})^6] \tag{22}$$

where ε is the minimum value of the potential function and σ is the distance when the potential is zero.

n-m potential:

$$U(r_{ab}) = \frac{E_0}{n-m}[m(\frac{r_0}{r_{ab}})^n - n(\frac{r_0}{r_{ab}})^m] \quad (23)$$

When the values of *n* and *m* are 12 and 6 respectively, the potential function becomes:

$$U(r_{ab}) = E_0[(\frac{r_0}{r_{ab}})^{12} - 2(\frac{r_0}{r_{ab}})^6] \quad (24)$$

where r_0 is the distance between the particles when the potential function has the minimum value E_0.

Buckingham potential:

$$U(r_{ab}) = A\exp(-\frac{r_{ab}}{B}) - \frac{C}{r_{ab}^6} \quad (25)$$

where *A*, *B* and *C* are constants that have different values for different types of particles (atoms, molecules or united units)

(II) Electrostatic (coulomb) potentials

The function to calculate the coulomb potential between two ions of charges is as follows:

$$U(r_{ab}) = \frac{1}{4\pi\varepsilon} \cdot \frac{q_a q_b}{r_{ab}} \quad (26)$$

1.5.3 DLPOLY file system

DLPOLY software uses input files to input data, including configuration data, control parameters and force field data. When the simulation is being done and finished, the results will be outputted in output files. Figure 1.3 shows these files.

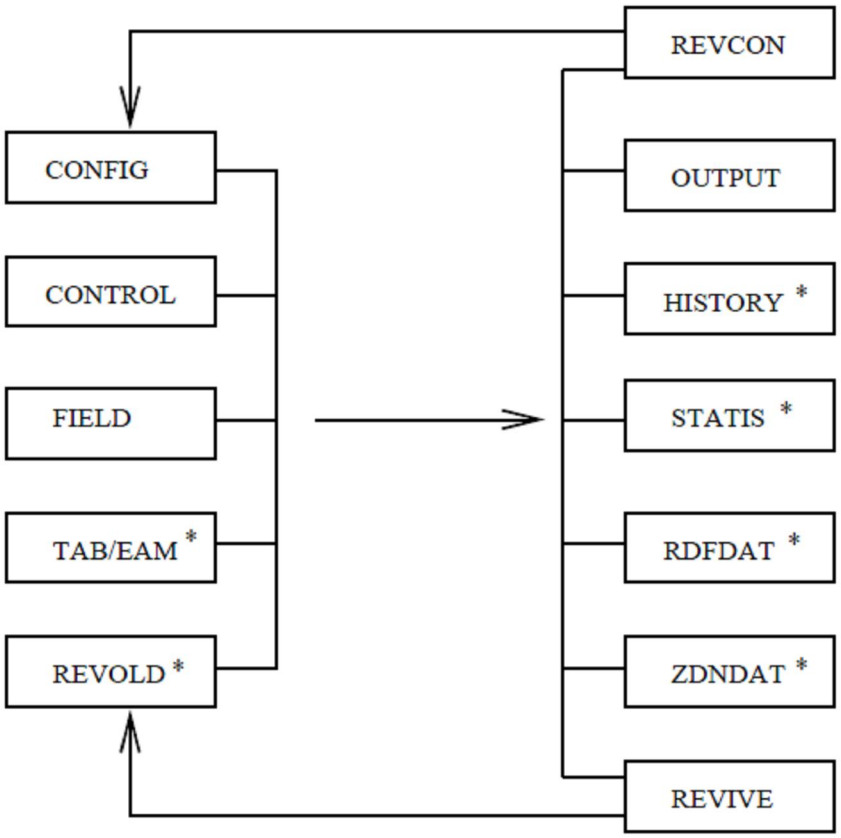

Figure1.3 The file systems of DLPOLY

1.6 Permeability, solubility and diffusivity modeling background

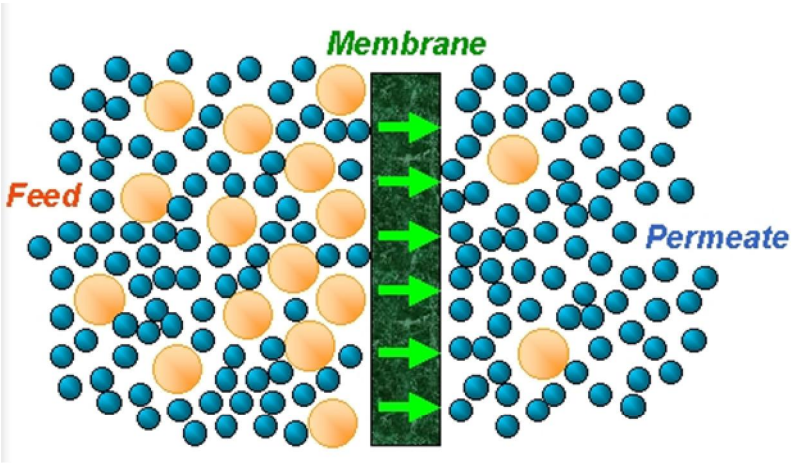

Figure 1.4 Schematic showing penetrants transport through a membrane

Figure 1.4 shows the penetrants transport through a membrane. Assume the pressure difference

between the two sides of the membrane is Δp and the thickness of the membrane is l, then the flux of certain type of penetrants through the membrane is:

$$q = P \cdot \frac{\Delta p}{l} \tag{27}$$

where P is the permeability of that type of penetrants. Therefore the permeability is used to compare transport properties of different penetrants.

The equation to calculate permeability is as follows [90-94]:

$$P = S \cdot D \tag{28}$$

where S and D represent solubility and diffusivity of penetrants in the membranes, respectively.

I now present how to predict solubility and diffusivity in the membranes of polymers and composites. Firstly, prediction of solubility (sorption equilibria) will be discussed.

Consider a mixture of c components indexed as 1, 2, … , c. Herein component 1 will be the polymer, while components 2, 3, … will be the penetrants whose permeation properties are of interest. In Figure 1.4, the sorption equilibria is between a fluid phase, consisting mainly of components 2,…,c, and a polymer phase containing all components. The fugacity of component i is denoted by f_i. The number of molecules, mole fraction and molecular weight of component i in the membrane phase are denoted with N_i, x_i and M_i, respectively. The symbol ρ_{molec} is used to denote the molecular density, the total number of molecules of all species per unit volume in the membrane phase. N_{Avo} represents the Avogadro constant.

If the polymer or composite phase can be regarded as completely not volatile or insoluble, and therefore absent from the gas fluid phase, it will be more convenient to consider the polymer/composite phase alone in the $N_1 f_2 f_3 ... f_C PT$ ensemble. In this ensemble, the total number of molecules of polymer/composite N_1, the fugacity of all gas molecules species f_i ($2 \le i \le c$), the temperature T and the pressure P are constant or fixed. Only c quantities

$f_2, f_3, ..., f_C, P, T$ are independent: If the gas fluid phase is pure, its fugacity can be obtained from P and T using an equation of state. Similarly, in a multicomponent fluid phase, $f_2, f_3, ..., f_C$ can be obtained from P, T and (c-2) mole fractions which determine the composition of the polymer/composite-free gas fluid phase. A probability density for the $N_1 f_2 f_3 ... f_C PT$ ensemble has been derived. The mean number of molecules $\langle N_i \rangle_{N_1 f_2 f_3 ... f_C PT}$ ($2 \le i \le c$) and the volume $\langle V \rangle_{N_1 f_2 f_3 ... f_C PT}$ ($2 \le i \le c$) of the polymer/composite phase, and therefore the molar densities of the penetrant species and the swelling of the polymer/composite because of sorption, will be conveniently obtained as ensemble averages with respect to this probability density.

The excess chemical potential of species *i* in the polymer/composite phase is defined as the chemical potential minus the chemical potential that species *i* would have as a pure ideal gas at the same temperature and molecular density:

$$\begin{aligned} &\mu_i^{ex}(\rho_{molec}, x_2, x_3, ..., x_c, T) \\ &= \mu_i(\rho_{molec}, x_2, x_3, ..., x_c, T) - \mu_{i,pure}^{ig}(\rho_{molec}, x_2, x_3, ..., x_c, T) \end{aligned} \tag{29}$$

The excess chemical potential is related to the fugacity f_i with the relation:

$$\mu_i^{ex} = RT \ln\left(\frac{\beta f_i}{\rho_{molec} x_i}\right) \tag{30}$$

where $\beta = 1/(k_B T)$ and $k_B = R / N_{Avo}$ is the Boltzmann constant. μ_i^{ex} can be obtained by the Widom test particle insertion method.

The solubility of component *i* in the polymer/composite phase can be defined as the slope of the line connecting the origin to a point ($f_i, \rho_{molec} x_i / N_{Avo}$) on the isotherm. Therefore, the solubility of a gaseous penetrant in the units of cm^3 (STP)/(cm^3 atm) can be obtained as:

$$S_i = \frac{22400 cm^3(STP)}{mol} \frac{\rho_{molec} x_i}{N_{Avo} f_i} \tag{31}$$

Combination of equations (31) and (30) gives the following equation:

$$S_i = \frac{22400 cm^3(STP)}{mol} \frac{1}{RT} \exp(-\frac{\mu_i^{ex}}{RT}) \tag{32}$$

According to the equation, determining μ_i^{ex} with the Widom test particle insertion method will give the value of solubility. From the relationship $S = K \cdot C_0$, one obtains

$$P = S \cdot D = K \cdot C_0 \cdot D \tag{33}$$

C_0 is the ideal gas concentration at standard condition and K is the solubility coefficient with its unit being 1, which is computed with equation (34):

$$K = \int_{-\infty}^{+\infty} d(\Delta E) \rho(\Delta E) e^{-\Delta E / RT} \tag{34}$$

where ΔE is the potential energy difference due to the insertion of penetrants and $\rho(\Delta E)$ is the probability density of the energy difference being ΔE. Most researchers [90-94] used this equation to calculate solubility of penetrants in matrices. However, researchers like Mueller-Plathe [90] noticed that the calculated results of solubility coefficients are much higher than the experimental results. Here in the work, activity coefficient is introduced to correlate the experimental and calculated results of solubility coefficients. Explanation of the deviation was also given.

When the penetrants enter the Fickian diffusive regime, the mean square displacement of penetrants averaged over different time origin can be employed to calculate diffusivity with the following equation [35, 95, 96]:

$$D = \lim_{\Delta t \to \infty} \frac{< [\underline{R}(t_0 + \Delta t) - \underline{R}(t_0)]^2 >}{6 \times \Delta t} \tag{35}$$

where $\underline{R}(t)$ is vector position of penetrants at time t and < > means an ensemble average.

According to equation (35), diffusivity may be determined with least square fit under the condition of large Δt. Furthermore the displacement must occur in the Fickian diffusive zone.

Otherwise, the calculated diffusivity will not be correct. That is because the penetrant transports have different characteristic and different time regions (15). In short time regions, the mean-square displacements follow a power law of t^2. In long time regions, when the penetrants enter the Fickian diffusive zone, the mean-square displacements are linear in time, where Einstein's equation (equation (35)) is applicable. At intermediate regions, anomalous diffusion is observed and the mean-square displacements obey a power law of $t^{0.5}$.

1.7 Objectives of the project

- Molecular dynamics simulation of penetrants transport in composite poly (4-methyl-2-pentyne) and silica nanoparticles;
- Comparing penetrants transport in composite poly (4-methyl-2-pentyne) and two forms of silica nanoparticles through molecular dynamics simulation;
- Determine the parameters of 'Ti' in the Lennard-Jones potential equation, simulate penetrants transport in composite poly (4-methyl-2-pentyne) and TiO_2 nanoparticles, and compare the results with composite poly (4-methyl-2-pentyne) and silica nanoparticles.

The details will be presented in the following sections.

Chapter 2

Molecular dynamics simulation of penetrants transport in composite poly (4-methyl-2-pentyne) and amorphous silica nanoparticles

2.1 Introduction

As described in Chapter 1, in industry the separation of methane from higher hydrocarbons, organic monomers from nitrogen and others are important processes. The application of these processes creates significant economical benefits. Furthermore, the separation of most waste gas mixtures not only gets useful gas from the mixture but also avoids environmental pollution. As a result, these processes also have significant environmental benefits. It is essential to develop and optimize these processes and therefore to do in-depth exploration of these processes.

In these processes, membranes made of composite material [2] are used due to their better performance than membranes, instead of membranes consisting of polymer solely. For example, the PMP and silica nanoparticle composite is used to separate C_4H_{10} (n-butane) from mixtures of C_4H_{10} and CH_4, H_2, etc.

Most MD simulation researches of transport property are focused on penetrants transport in polymer, blends, or ceramics. However, to our knowledge, few researchers have explored the

transport property of penetrants in composites using MD simulation. Smith, et. al [2] only simulated the properties of an imaginary model composite system. Generally, the structure of the composites of a polymer and nanoparticles is complex. Herein the composite structure was created and MD simulation was done based on the structure created successfully.

Firstly, the structure of the PMP and silica nanoparticle composite was established. Using the structure, the cavity size distribution was analyzed. The diffusivity of different penetrants, including H_2, O_2, Ar, CH_4 and n-C_4H_{10} was determined through least square fit of displacement at different times in the Fickian diffusive regime. Based on the resistance concept in heat and mass transport, an equation was formulated to correlate the diffusivity of the same penetrants in different materials. The solubility coefficients and the permeability of different penetrants in PMP and the composite were calculated. The distribution of potential difference due to the penetrant insertion was analyzed in detail. The details of the research and the corresponding results will be presented in the following sections.

2.2 Polymer (PMP) model

Like Tamai et. al. [35], the PMP sample is modeled as $H(CCH_3CC_3H_7)_{31}H$. The methyl (including the methyl in propyl) groups are taken as united groups, while H and C are treated as individual units. The density of PMP at 300K was used to determine the cell size. The molecular weight of one chain is 2606. In the simulation the AMBER/OPLS force field [97, 98] was used. The electrostatic interaction was computed using the Ewald Sum [89] algorithm. The VDW interaction was computed with the Lennard-Jones equation [89].

The generally employed self-avoid random walk algorithm [99] was employed to create the initial structure of PMP. The chains were folded when the periodic boundary condition was employed. 5000 steps of energy minimization were performed according to steepest descent algorithm to obtain a reasonable starting configuration. This was followed by 3 ns MD

production run. According to the research results of Van der Vegt [100], the production run time can be estimated approximately from the distance traveled by the penetrant in one diffusive jump (l_{jump} , equal to 0.5-1nm) according to the following equation:

$$t = \frac{l_{jump}^{\ 2}}{6 \times D} \tag{36}$$

The structure of the relaxed PMP chains is presented in Figure 2.1.

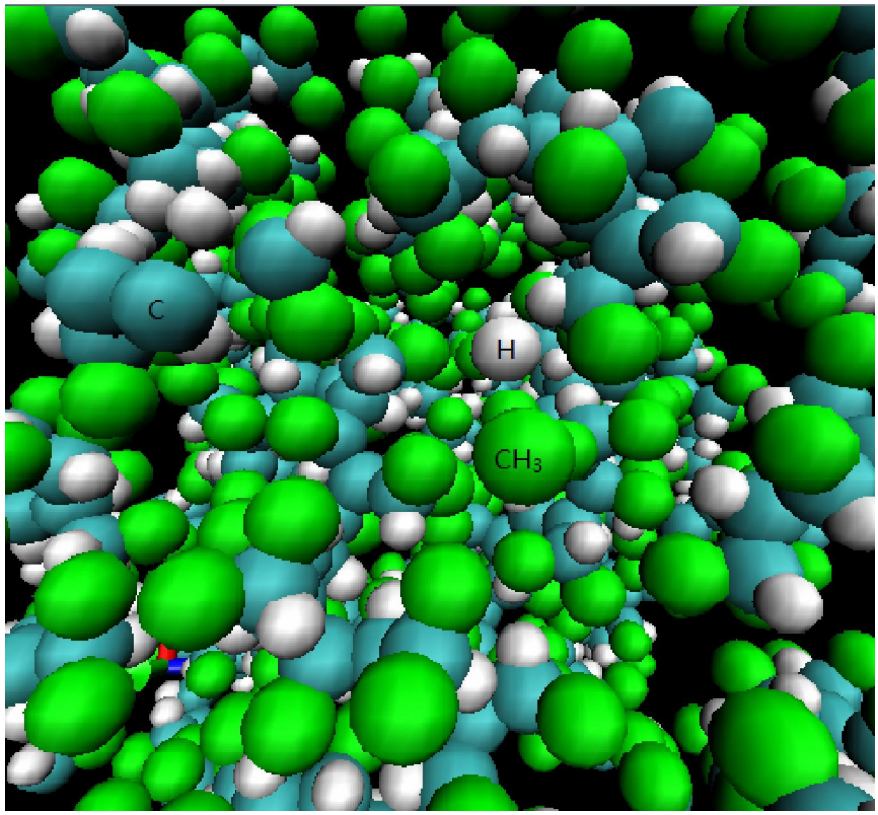

Figure 2.1: The relaxed structure of PMP

2.3 Silica nanoparticle

The diameter of the nanoparticle is 2.5 nm. The structure of the amorphous silica nanoparticle presented in Figure 2.2. The structure is similar to diamond. According to equation (36), because diffusivity of penetrants in silica is higher than in the PMP, the

corresponding production time needed to simulate the diffusion should be shorter.

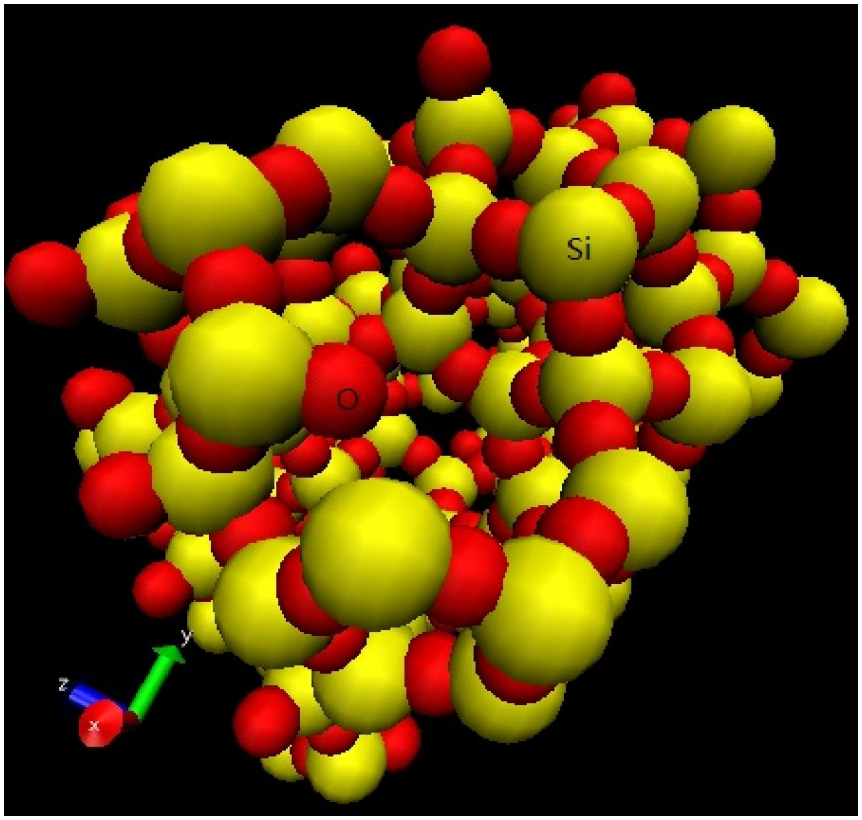

Figure 2.2: Structure of silica nanoparticle

2.4 PMP and silica nanoparticle composite

In the composite, the silica nanoparticle is placed among the chains in the cell. The simulated system was composed of 5 chains and 1 nanoparticle. Figure 2.3 shows the relaxed structure of the composite system. Finally, to explore the influence of nanoparticle mass fraction on transport, other systems listed in Table 2.1 were simulated.

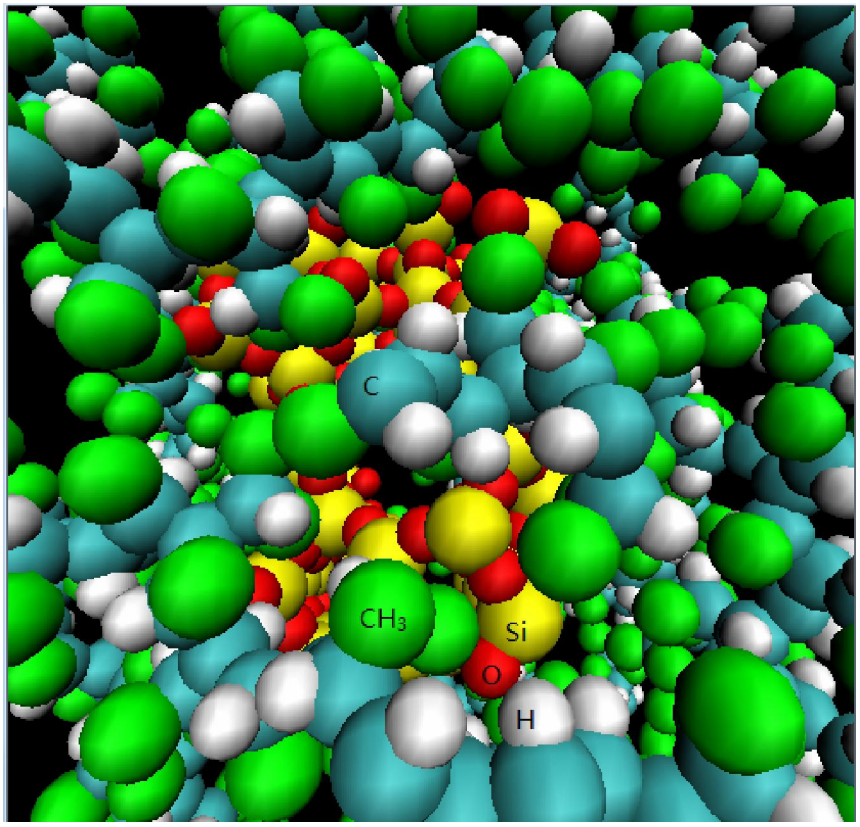

Figure 2.3: The relaxed structure of the PMP and silica nanoparticle composite

Table 2.1: The number of nanoparticles and chains, the corresponding mass fraction of nanoparticles and the cell volume for different simulation systems

Mass fraction of nanoparticles	Number of chains	Number of nanoparticles	Cell volume (nm^3)
0.232	7	1	44.748
0.297	5	1	34.300
0.320	9	2	63.376
0.346	8	2	58.152
0.384	7	2	52.929
0.467	5	2	42.481

2.5 Penetrants

The coarse-grained united-atom model is employed to describe the gas molecules. H_2, O_2, CH_4 and Ar are all treated as single group. n-C_4H_{10} is regarded as consisting of two methyl

groups and two methylene groups. The Lennard-Jones equation is employed to calculate VDW interactions. The Lennard-Jones parameters are listed in Table 2.2. [35, 95, 99, 101, 102] For interactions between different types of units, the Lorentz–Berthelot mixing rule is used.

Table 2.2: Lennard-Jones parameters of different penetrants and silica atoms

Penetrant	LJ ε (kcal/mol)	LJ σ (nm)
H_2 [101]	0.0752	0.232
O_2 [101]	0.0885	0.309
CH_4 [35, 99, 37]	0.294	0.373
Ar [95]	0.237	0.341
$CH_3(C_4H_{10})$ [35, 98, 100]	0.175	0.391
$CH_2(C_4H_{10})$ [35, 102]	0.117	0.391
Si [35, 99]	0.584	0.338
O [35, 99]	0.203	0.296

It should be noted that the gas molecules should be inserted before energy minimization is performed. Otherwise, if the penetrants are inserted after the energy minimization run of the PMP or composite structure, since gas molecules cause the system to lose relaxation due to the additional interaction between the gas molecules and the matrix, a second energy minimization must be done; 7 molecules are inserted in every simulation.

2.6 Other simulation details (parameters)

The DLPOLY (21) software package was employed herein. The Verlet algorithm [89] was used to solve equations of motion with time step of 1.5fs under constant pressure and temperature condition. All the simulations were conducted in the NPT ensemble. The weak coupling technique [89] was used to modulate the T and P with relaxation times of 0.1ps and 0.5ps, respectively. The temperature was set to 300K. The pressure was 1.0 bar. Transport usually occurs at such temperature and pressure. The VDW interaction potentials were cut off at 1.2 nm. The electrostatic interaction potential cut off distance was also 1.2 nm. The time for production run was set as 3ns for diffusion in PMP and PMP and silica nanoparticle composite or set according to equation (36). When the time for the production run was set as 10ns, the

results coincided with that of a production run time of 3ns. So 3ns is long enough to give good results. The VDW interaction potentials were cut off at 1.2 nm. If they were cut off at shorter distance, the calculation results will not be precise enough. If they were cut off at longer distance, waster of computation time will be caused with no improvement of precision.

2.7 Determination of diffusivity

When the penetrants enter the Fickian diffusive regime, the mean square displacement of penetrants averaged over different time origin can be employed to calculate diffusivity with equation (35) [35, 95, 96] . According to equation (35), diffusivity may be determined with least square fit under the condition of large Δt . Furthermore the displacement must occur in the Fickian diffusive zone.

2.8 Calculation of solubility

In the mass transport process, the permeability is widely used to compare transport properties of different penetrants [103]. The equation to calculate permeability is as follows [90-94]:

$$P = S \cdot D = K \cdot C_0 \cdot D \tag{33}$$

where P and S represent permeability and solubility of penetrants, respectively. C_0 is the ideal gas concentration at standard condition and K is the solubility coefficient with its unit being 1, which is computed with equation (34):

$$K = \int_{-\infty}^{+\infty} d(\Delta E)\rho(\Delta E)e^{-\Delta E / RT} \tag{34}$$

where ΔE is the potential energy difference due to the insertion of penetrants and $\rho(\Delta E)$ is the probability density of the energy difference being ΔE . The integration in equation (4) gives the ensemble average of $e^{-\Delta E / RT}$. It may be discretized as Widom presented [90, 104, 105].

The Widom test particle insertion method [104, 106] is employed to calculate the solubility coefficients. Assume the particle is inserted into the system randomly and the potential change due to the penetrant insertion is ΔE_k . If N times of insertions are done and N is large enough, then the solubility coefficient can be determined with equation (37).

$$K = \frac{\sum_{k=1}^{N} e^{-\Delta E_k / RT}}{N} \tag{37}$$

The author noticed that equation (33) holds only when the composition of penetrants in matrices is low. When the composition of penetrants in matrices is high, the activity coefficient of penetrants would differ from 1. Assume the gas phase is ideal gas at standard condition and the fugacity of penetrants in matrices can be computed according to Henry's theory.

$$f_g = p_0 = R \cdot T \cdot C_0 \tag{38}$$

$$f_m = H \cdot x \cdot \gamma = H \cdot \frac{C_m \cdot M_P}{m_t} \cdot \gamma \tag{39}$$

where C_m stands for the molarity of penetrants in the matrices, M_P represents the molecular weight of penetrants and m_t represents the total mass of both penetrants and the matrices. The weight fraction concentration of penetrants, x, is $\frac{C_m \cdot M_P}{m_t}$ in both pure PMP and the composite. The difference is that in the composite, the total mass includes the mass of nanoparticles, besides that of penetrants and PMP.

At equilibrium, the fugacity of penetrants in the gas phase and the matrix phase should be equal, so equation (40) will be obtained:

$$K = \frac{C_m}{C_0} = \frac{R \cdot T \cdot m_t}{H \cdot \gamma \cdot M_P} \tag{40}$$

The activity coefficient γ is one when the solution of penetrants in matrices is infinitely

dilute. When the Widom test particle insertion method is employed to calculate solubility coefficient, the composition of penetrants is low. Assume the corresponding γ can be regarded as one and equation (40) becomes:

$$K_{cal} = \frac{C_m}{C_0} = \frac{R \cdot T \cdot m_t}{H \cdot M_P} \tag{41}$$

According to equation (41), Henry's constant can be computed with the following equation

$$H = \frac{R \cdot T \cdot m_t}{K_{cal} \cdot M_P} \tag{42}$$

The experimental results are obtained when the penetrants compositions in the matrices reach C_m ; so according to equations (33), (40) and (41), the experimental values and the calculated values of permeability satisfy equation (43):

$$P_{cal} = P_{\exp} \cdot \gamma(C_m) \tag{43}$$

When the composition of penetrants in the matrices increases, the activity coefficient will deviate from one and consequently the calculated values of permeability will deviate from the experimental values.

2.9 Results

The simulation results will be shown in the section.

2.9.1 Cavity size distribution

The cavity size distribution is presented in Figure 2.4. The number of cavities with radius in a certain narrow ranges $(r, r + \Delta r)$ was counted first. The counted cavities number $N(r)$ divided by the total number of cavities over the whole range, N_t , and radius range width, Δr , will give the probability density, $P(r)$, in Figure 2.4. That is:

$$P(r) = \frac{N(r)}{N_t \cdot \Delta r} \tag{44}$$

From these figures, it is observed that in the PMP and silica nanoparticle composite, ratio of large cavity is higher than in pure PMP. Therefore, due to the existence of the silica nanoparticle, the cavity size distribution varies significantly, which lead to higher diffusivity in the composite.

2.9.2 Diffusivity calculation

The trajectories of CH_4 in PMP and in the PMP and silica nanoparticle composite are presented in Figure 2.5. I have calculated the cavity size distributions at 100 different simulation moments. The standard deviations of distributions corresponding to different cavity sizes are presented in Table 2.3. The mean relative standard deviation is 3.18%.

Table 2.3: The standard deviations of distributions corresponding to different cavity sizes

Cavity radius (angstrom)	1.0	1.5	2.5	3.0	3.5	4.0	4.5	5.0
Standard deviation (×0.01)	0.930	1.350	0.601	0.510	0.318	0.204	0.186	0.154
Relative standard deviation(%)	3.10	3.37	2.40	3.40	3.53	2.91	3.39	3.42

Figure 2.5 is to show the position of the molecules at hundreds of different moments. In the research, the united-atom model is employed to describe the methane molecule. As a result, a methane molecule is regarded as a particle without bonds. Most researchers used figures like Figure 2.5 to show the trajectory of particles.

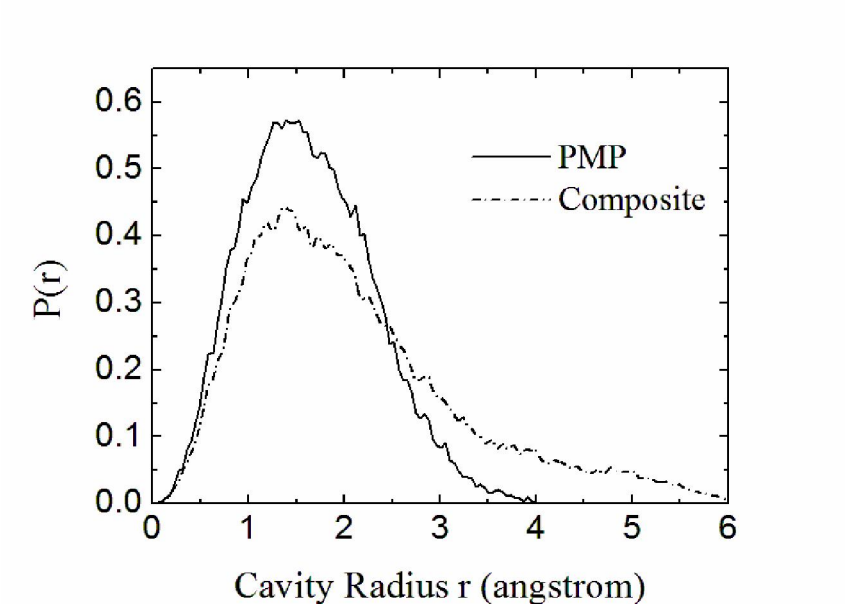

Figure 2.4. The cavity size distribution in PMP and in the PMP/silica nanoparticle composite. P(r) is the probability density of the cavity radius being r.

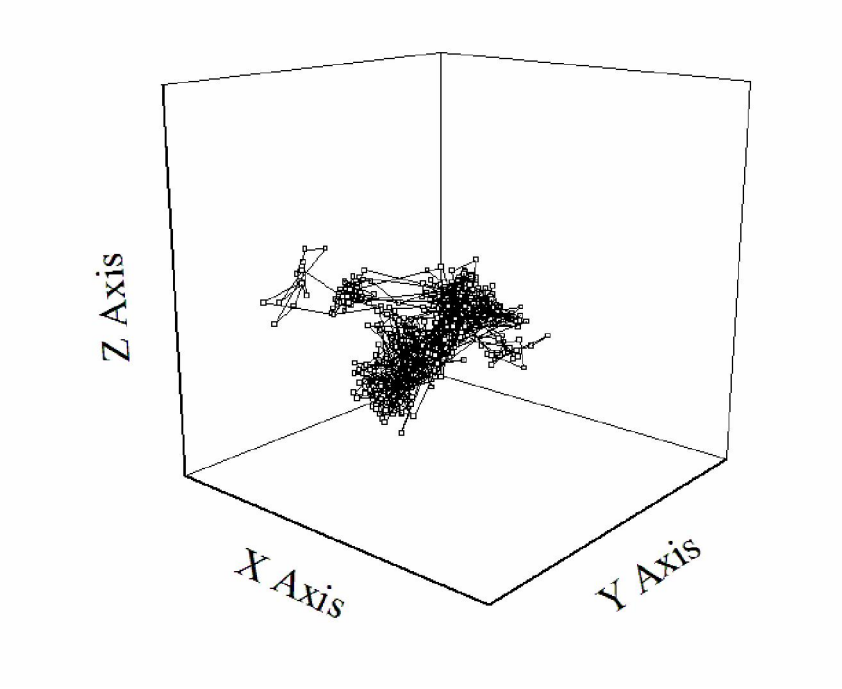

(a)

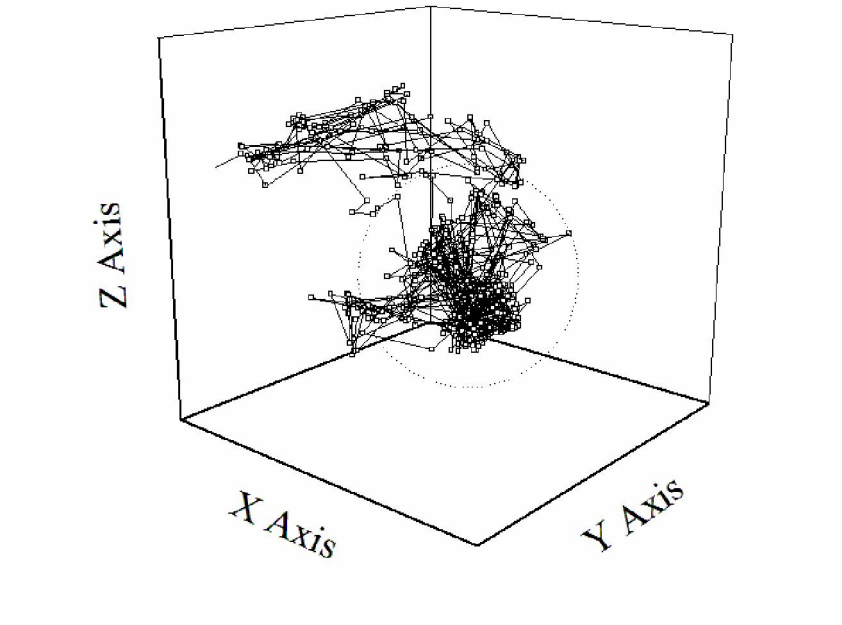

(b)

Figure 2.5. The trajectory of CH_4 in (a) PMP; (b) the PMP and silica nanoparticle composite (the time interval between two adjacent points along the trajectory is 3ps). The circle in (b) represents the position of the nanoparticle.

It is observed from these figures that because the ratio of large cavity in the composite is

higher than in the pure PMP, the penetrants travel in a larger region in the composite than in the pure PMP. In the composite, the penetrants move around the whole cell, not only in the PMP portion of the cell. It was my view that penetrants could not pass through these nanoparticles dispersed in the composite and only travel in the PMP portion of the composite because of the influence of the interface between the PMP and the silica nanoparticle. The MD simulation illustrated clearly that penetrants travel in both portions of the composite.

The logarithmic plot of mean square displacement averaged over different time origin versus time was used to determine if the transport is in the Fickian diffusive regime. Subsequently the values of the diffusivity were determined via the slope of the line obtained from a least squares fit.

Figure 2.6 shows the relationship between the mean square displacement and the simulation time. Results of CH_4 diffusion in both PMP and the PMP and silica nanoparticle composite are presented.

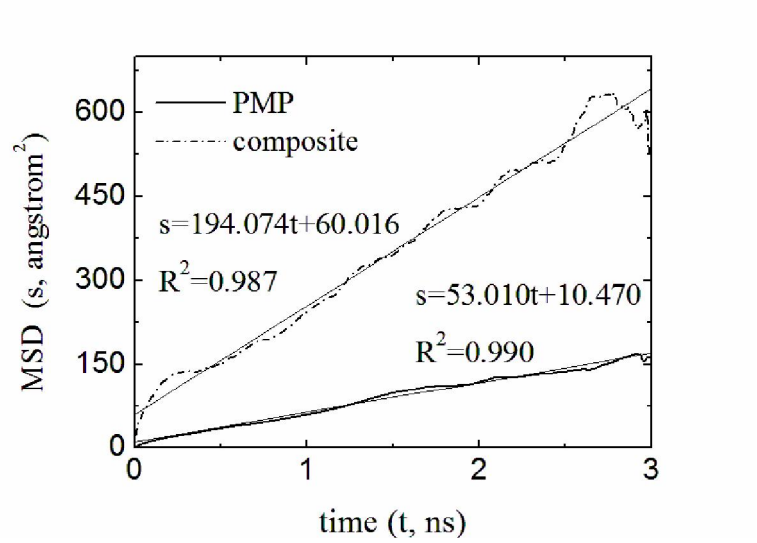

Figure 2.6. The relationship between the mean square displacement averaged over different time origin and simulation time. R^2 is the square of correlation coefficient.

The simulation results of diffusivity of different penetrants in PMP, zeolite and PMP and

silica nanoparticle composite are presented in Table 2.4.

Table 2.4: Diffusivity of penetrants in composite, PMP and zeolite ($D \times 10^9 m^2/s$). The data in the parenthesis is the standard deviation. *CMP* represents composite. *ZEO* stands for zeolite

Diffusivity / Penetrants	D_{PMP}	D_{ZEO}	D_{CMP}	$\frac{1}{D_{PMP}} - \frac{1}{D_{ZEO}}$	$\frac{1}{D_{CMP}} - \frac{1}{D_{ZEO}}$
H_2	47.5(16)	1150(230)	123.1(35.2)	0.020	0.00726
O_2	0.610(0.17)	63(10)	5.56(3)	1.623	0.164
Ar	0.166(0.07)	487(32)	0.825(0.3)	6.022	1.210
CH_4	0.092(0.05)	436(40)	0.323(0.13)	10.867	3.094
n-C_4H_{10}	0.030(0.02)	256(36)	0.101(0.06)	33.329	9.897

From Table 2.4 it is observed that from H_2, O_2, CH_4, Ar to n-C_4H_{10}, the corresponding diffusivity in PMP decreases. This trend matches the changing trend of the diffusivity of these penetrants in polyethylene [92, 93, 107, 108].

When heat is conducted through two layers of different materials, the overall heat transport equation is as follows:

$$\frac{1}{K} = \frac{l_1/(l_1+l_2)}{k_1} + \frac{l_2/(l_1+l_2)}{k_2} \tag{45}$$

where K is the overall heat conductivity, k_1 is the heat conductivity of the first heat conduction layer, l_1 is the thickness of the first layer, k_2 is the heat conductivity of the second heat conduction layer and l_2 is the thickness of the second layer.

Based on equation (45), an equation was developed to correlate the diffusivity of the same penetrants in different materials. The equation is:

$$\frac{1}{D_{CMP}} - \frac{1}{D_{ZEO}} = a\left(\frac{1}{D_{PMP}} - \frac{1}{D_{ZEO}}\right) + b \tag{46}$$

The least square fit (Figure 2.7) was employed to determine the parameters *a* and *b*. From Figure 2.7, it is observed that the value of *a* is 0.303 and *b* is -0.248. The square correlation coefficient is close to 1. The equation is applicable to predict the approximate value of

diffusivity in composite with diffusivity values in pure PMP and zeolite.

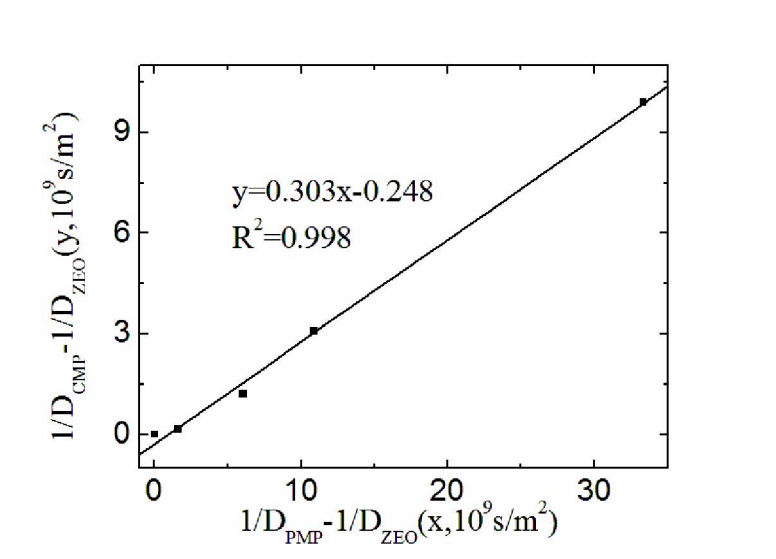

Figure 2.7: Least square fit to determine the parameters *a* and *b*

2.9.3 Computation of solubility coefficients and permeability

During the production run, the PMP structures and the composite structures have minor variation due to minor oscillation of atoms around their equilibrium positions. As a result, the values of the computed solubility coefficients at different production time would fluctuate. To get suitable results for the solubility coefficients, the values of the solubility coefficients corresponding to structures at different time with certain interval were calculated first. Then the average value of all the coefficients obtained would be regarded as the solubility coefficients of the corresponding penetrants in that material. The solubility coefficients of CH_4 in PMP and PMP and silica nanoparticle composite at different time are presented in Figure 2.8.

The solubility coefficients calculation results of different penetrants in PMP and composite are listed in Table 2.5. The weight concentration of penetrants in PMP is $\frac{m_{penetrants}}{m_{penetrants}+m_{PMP}}$,

while that in composite is $\frac{m_{penetrants}}{m_{penetrants} + m_{PMP} + m_{NP}}$.

Form Table 2.5 it is observed that from H_2, O_2, Ar, CH_4 to n-C_4H_{10}, the corresponding solubility coefficients decreases. This trend matches the changing trend of the solubility values of these penetrants in polyethylene [92].

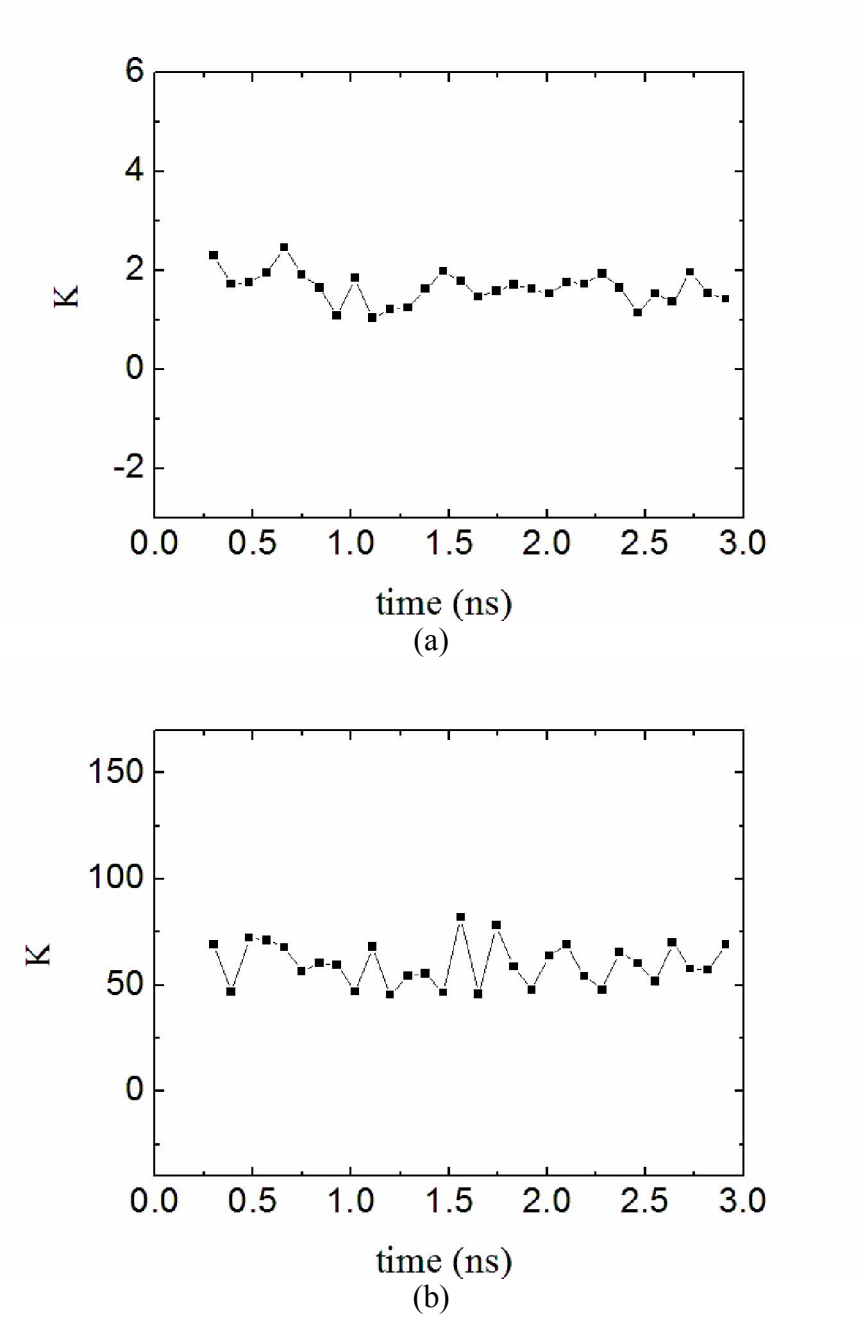

Figure 2.8. The solubility coefficients of CH_4 in different (a) PMP structures corresponding to different time; (b) composite structures corresponding to different time

Table 2.5. The solubility coefficients calculation results of different penetrants in PMP and the composite. The data in the first parenthesis are the standard deviation; the data in the second parenthesis of each cell are weight concentration of the penetrants. The units are all 1.

penetrants \ matrix	PMP	Composite
H_2	0.250 (0.063) (0.0000459)	0.610 (0.110) (0.0000606)
O_2	0.269 (0.117) (0.000790)	1.165 (0.232) (0.00185)
Ar	0.838 (0.216) (0.00307)	10.853 (2.791) (0.0216)
CH_4	1.654 (0.323) (0.00243)	59.986 (10.036) (0.0477)
n-C_4H_{10}	107.304 (24.167) (0.363)	5876.651 (2037.85) (0.876)

To explore the distribution of potential difference due to the penetrant insertion, 10000 successive random insertions were done in the matrix structure corresponding to 2.5ns in Figure 2.8. The calculation results show that among these 10,000 random insertions, 402 insertions have negative potential change. In the composite, the potential change (ΔE) is composed of two parts, namely (a) the interaction potential (ΔE_{PMP}) between the inserted penetrant and the PMP chains units and (b) the interaction potential (ΔE_{NP}) between the penetrant and the nanoparticle Si and O atoms. Figure 2.9(a) shows the potential difference of the 402 insertions. The label number *i* means that the corresponding potential difference is the *i*th lowest potential difference. The contribution of each insertion is proportional to $e^{-\Delta E / RT}$. Figure 2.9(b) shows the values of $e^{-\Delta E / RT}$ for the 402 insertions. The 20 insertions with the 20 lowest potential change account for 99% of the contributions of all the insertions. Figure 2.9(c) presents the potential difference and the corresponding interaction potential between inserted particle and the atoms of the nanoparticles for the 20 insertions with the 20 lowest potential differences. It is observed that interaction potential between the inserted penetrant and the Si and O atoms of the nanoparticles contributes much to the potential difference due to the penetrant insertion. The mean value of the ratio of ΔE_{NP} to ΔE for the 20 insertions is over 93%. Therefore, it is the interaction between nanoparticle and penetrants that lead to the higher

solubility in composite, not because of the shape change of PMP chains, as some researchers tend to think[6]. The simulation results show that the trans conformation to gauche conformation ratio of PMP chains in PMP is 93:7 (±2), while that ratio in the composite is 87:13 (±2). The change in the ratio is insignificant. The trans to cis ratio of PMP chains is 99:1 (±1) in both PMP and the composite.

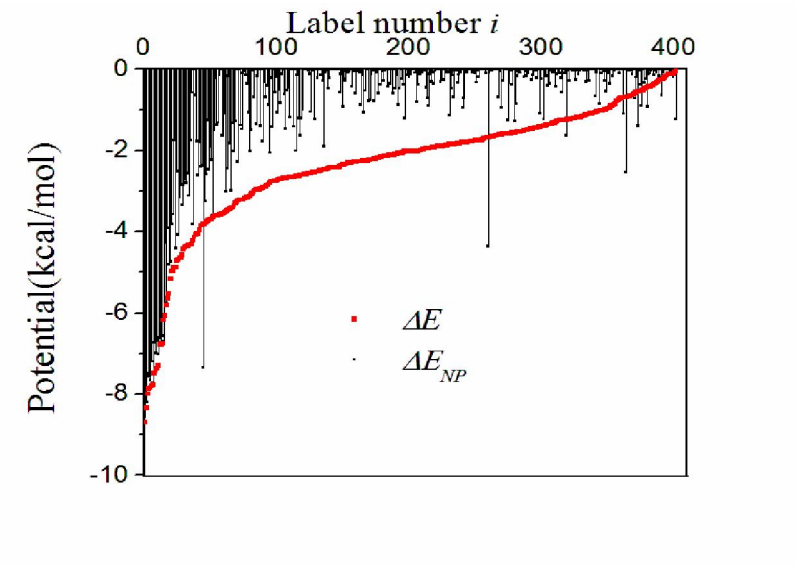
Label number i
0
100
200
300
400
0
-2
-4
-6
-8
-10
Potential(kcal/mol)
ΔE
ΔE_NP

(a)

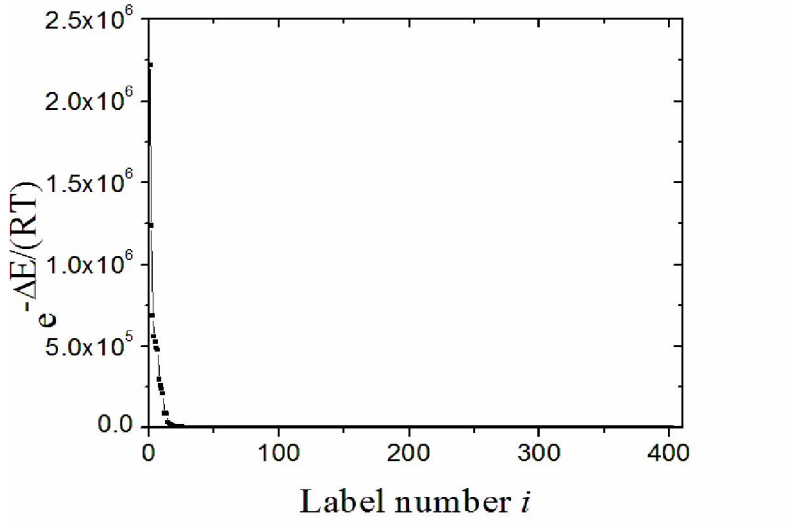
2.5x10^6
2.0x10^6
1.5x10^6
1.0x10^6
5.0x10^5
0.0
e^-ΔE/(RT)
0
100
200
300
400
Label number i

(b)

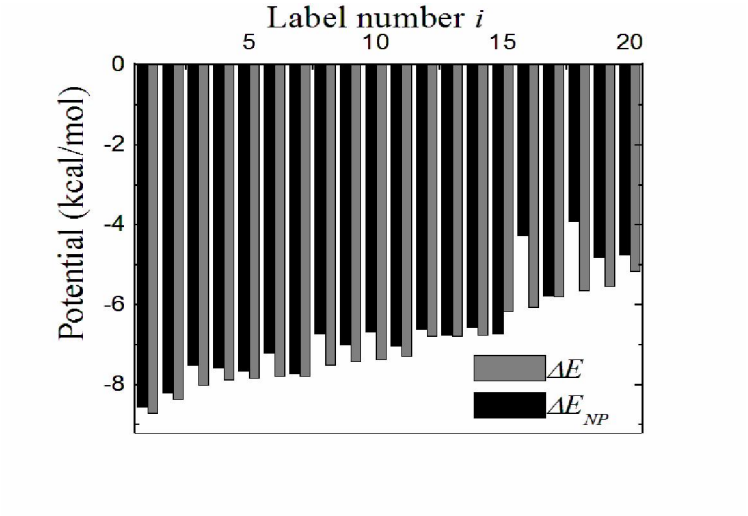

(c)

Figure 2.9 (a) the potential difference of the 402 insertions with negative potential change; (b) the values of $e^{-\Delta E/RT}$ for the corresponding 402 insertions in (a); (c) ΔE_{NP} and ΔE for the 20 insertions with the 20 lowest potential differences. The label number i means that the corresponding potential difference is the ith lowest potential difference.

Then with values of diffusivity and solubility coefficients, the permeability values of different penetrants in PMP and PMP and silica nanoparticle composite were calculated and listed in Table 2.6.

Table 2.6: The calculated permeability of different penetrants in PMP and composite

penetrants \ matrix	PMP			Composite
	Cal. (10^3 *barrer*)	Exp. (10^3 *barrer*)	γ	(10^3 *barrer*)
H_2	15.623	-	-	98.792
O_2	0.216	0.185(39, 44)	1.167	8.522
Ar	0.183	-	-	11.780
CH_4	0.203	0.191 (45)	1.068	25.479
n-C_4H_{10}	4.236	2.735 (45)	1.549	780.878

It is observed from Table 2.6 that the calculated permeability of O_2 and CH_4 is closer to the experimental values than the computed permeability of n-C_4H_{10}. From Table 2.5 it is observed

that the solubility of n-C_4H_{10} is high in PMP compared with O_2 and CH_4. The activity coefficient of n-C_4H_{10} in PMP will differ more from one than that of O_2 and CH_4 in PMP. Therefore the calculated permeability of n-C_4H_{10} in PMP will differ more from the corresponding experimental values than of O_2 and CH_4 in PMP.

Table 2.6 shows that the composite has high permeability compared with PMP for the same penetrants. Especially for n-C_4H_{10} the insertion of silica nanoparticle in PMP significantly increases permeability. The selectivity of n-C_4H_{10} over CH_4 increases from 20 to 31 due to the insertion of silica nanoparticles in PMP. The selectivity of n-C_4H_{10} over CH_4 is the permeability ratio between n-C_4H_{10} and CH_4. The PMP and silica nanoparticle composite is widely employed to separate the mixture of n-C_4H_{10} with other gas molecules in industry [103, 109].

2.9.4 The influence of nanoparticle mass fraction on selectivity

The CH_4 and n-C_4H_{10} transport in other systems listed in Table 2.1 has been simulated with MD method as well. Figure 2.10 gives the approximate relationship between the selectivity of n-C_4H_{10} over CH_4 and the weight concentration of nanoparticle in composite. The selectivity increases with the increase of weight concentration of nanoparticle. When the weight concentration is smaller than 0.232, the selectivity also decrease with the decrease of weight concentration until the selectivity reaches minimum when composite becomes pure PMP. Figure 2.10 can be employed to guide composite material and membrane design.

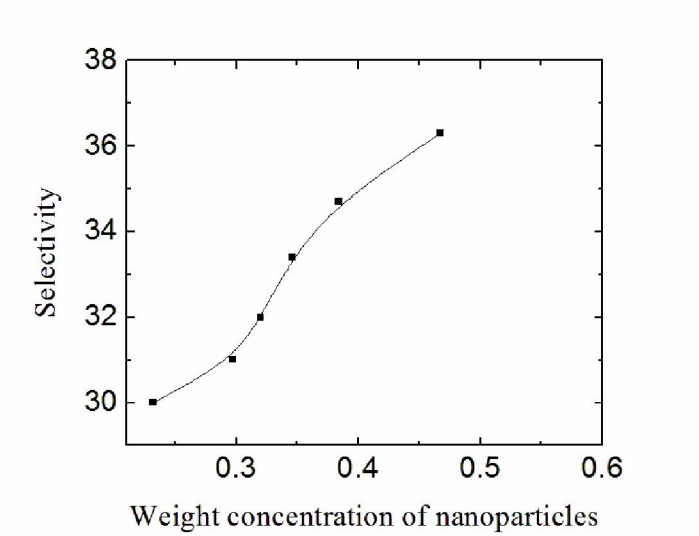

Figure 2.10. The relationship between the selectivity of n-C_4H_{10} over CH_4 and the weight concentration of nanoparticle in composite

2.9.5 Conclusion

From our knowledge, few researchers have explored the transport property of penetrants in composites using MD simulation. In this work, the structure of the PMP and silica nanoparticle composite was established. With the structure, the cavity size distribution was analyzed and it was observed that in the PMP and silica nanoparticle composite, larger cavities exist than in pure PMP, which contribute to the increase in diffusivity in the composite than in pure PMP. The diffusivity of different penetrants, including H_2, O_2, Ar, CH_4 and n-C_4H_{10} was determined through least square fit of the data of mean square displacement at different time in Fickian diffusive regime. The results show that from H_2, O_2, CH_4, Ar to n-C_4H_{10}, the corresponding diffusivity in PMP decreases. This trend matches the changing trend of the diffusivity of these penetrants in polyethylene. Based on the resistance concept in heat and mass transport, an equation was designed to correlate the diffusivity of the same penetrants in different materials. The equation can be employed to predict diffusivity in the composite with the diffusivity values in PMP and zeolite. The solubility coefficients and the permeability of different

penetrants in PMP and the composite were calculated. The distribution of potential difference due to the penetrant insertion was analyzed in detail. The results show that it is the interaction between Si and O atoms of the nanoparticle and penetrants that lead to the higher solubility in composite, not because of the shape change of PMP chains. Because the solubility of n-C_4H_{10} is high in PMP compared with O_2 and CH_4, the activity coefficient of O_2 and CH_4 will be closer to one than that of n-C_4H_{10} and the calculated permeability of O_2 and CH_4 is closer to the experimental values than the computed permeability of n-C_4H_{10}. Finally, the influence of weight concentration of nanoparticles on penetrants transport was explored. According to the simulation results, the selectivity of n-C_4H_{10} over CH_4 increases with the increase of mass fraction of nanoparticle.

Chapter 3

Comparing penetrants transport in composite poly (4-methyl-2-pentyne) and two forms of silica nanoparticles through molecular dynamics simulation

3.1 Introduction

In the production of natural gas, raw gas is treated to separate butane and higher hydrocarbons from methane in order to bring the heating value and the dew point to pipeline specification, and to recover the valuable higher hydrocarbons as chemical feedstock. Similarly, approximately 1% of the 30 billion lb/year of monomer used in polyethylene and polypropylene production is lost in nitrogen vent streams from resin purge operation. Recovery of these monomers would save US producers about $100 million/year.

Silica has different crystalline forms. In cristobalite, the Si and O atoms are so densely packed that there are probably no pores through which penetrants can pass, while in faujasite crystalline form, there exits pores that are probably large enough to allow penetrants to pass through. Amorphous silica may contain a mixture of small and large pores. In my previous work[3], the composite is composed of PMP and nanoparticle of amorphous silica. However, the transport properties of penetrants in the PMP and cristobalite silica nanoparticle composite (PMPC) and the PMP and faujasite silica nanoparticle composite(PMPF) are different. It is

essential to explore the reasons that lead to the difference; this knowledge would aid the design of membrane made of PMP and silica nanoparticles composite. Based on my previous work[3], the transport of different penetrants in PMPC and PMPF, was simulated and compared.

Molecular dynamics (MD) simulation is extensively employed to explore the transport properties of penetrants in organic polymers and inorganic materials. To my knowledge, few researchers have explored the transport property of penetrants in composites using MD simulation. The structure of the composites of a polymer and nanoparticles is generally complex. In the work, the PMPC and PMPF structures were created, relaxed and gas permeation simulation was done via MD.

I employed the logarithmic plot of mean square displacement averaged over different time origin versus time to determine if the transport is in the Fickian diffusive regime[4-6]. Subsequently values of the diffusivity were determined through the slope of the line obtained from a least squares fit. Finally, the solubilities and permeabilities of different penetrants, including H_2, O_2, CH_4, Ar and C_4H_{10} PMPC and PMPF were obtained.

3.2 Computational method

The PMP sample is modeled as $H(CCH_3CC_3H_7)_{31}H$, the same as aim 1.

The diameter of the nanoparticle is 2.5 nm. The structures of both the cristobalite silica and the faujasite silica are presented in Figure 3.1. The structures differ significantly. The silica of the faujasite form has pores that probably allow penetrants to easily pass through. The Si and O atoms of cristobalite silica are packed densely compared with the faujasite silica. The simulated 2.5nm faujasite silica nanoparticle contains 92 SiO_2 units, while the cristobalite silica nanoparticle is made up of 172 SiO_2 units.

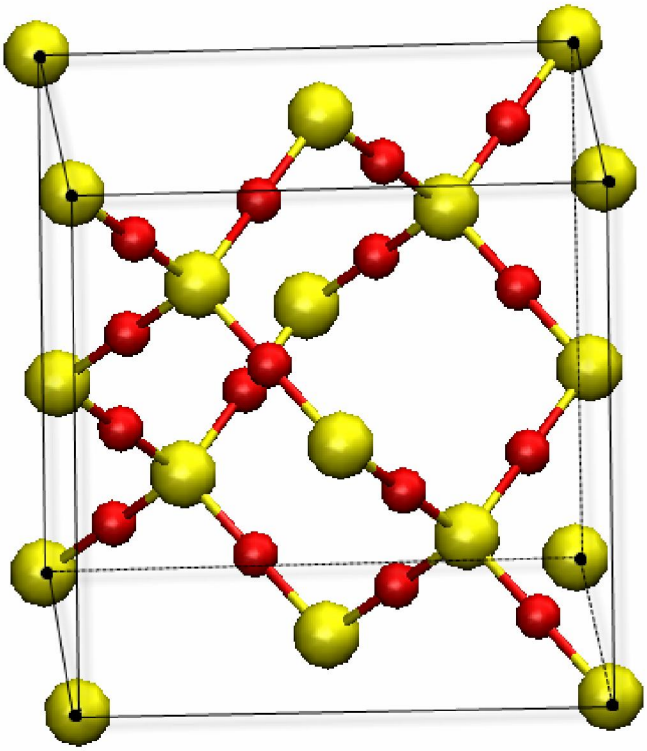

(a)

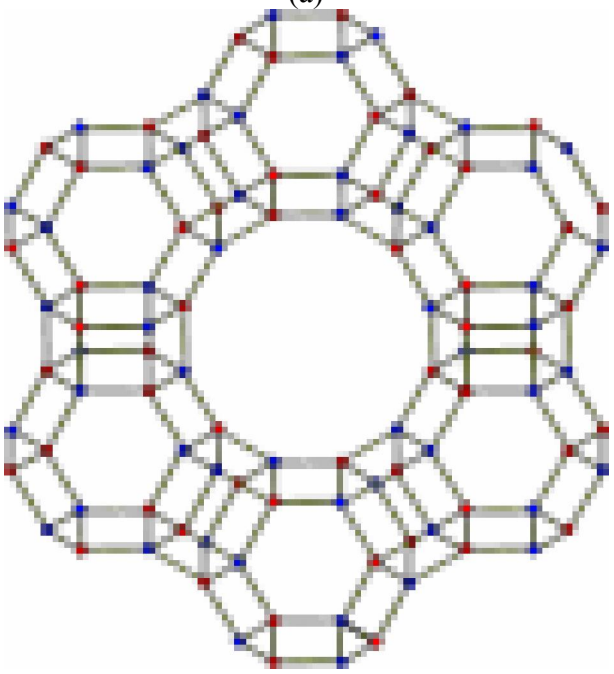

(b)

Figure 3.1: The structures of the cristobalite (a) silica and the faujasite (b) silica

In the composite, the nanoparticle is placed in the center of the simulation cell, among the PMP chains. The simulated systems were composed of 5 chains and 1 nanoparticle. Because the volume of the nanoparticles of both the cristobalite (a) form and the faujasite form is the same, the cell volume of both systems is the same, namely 34.3nm^3.

In Chapter 2, it has been stated that when the penetrants composition in matrices reaches C_m, the experimental values and the calculated values of permeability satisfy equation (43). When the composition of penetrants in matrices increases, the activity coefficient will differ more from one; in addition the calculated values of permeability will differ more from the experimental values.

If two types of penetrants, 1 and 2, are transported in matrices, the calculated selectivity of penetrant 1 over 2, without considering activity coefficient, would be

$$Sel_{cal} = \frac{P_{cal,1}}{P_{cal,2}} \tag{47}$$

while the experimental value of selectivity of penetrant 1 over 2, according to equation (43), should be

$$Sel_{\exp} = \frac{P_{cal,1}}{P_{cal,2} \cdot \gamma_1} \tag{48}$$

This assumes that the solubility of penetrant 2 is small and the corresponding activity coefficient can be regarded as 1. Here γ_1 is the activity coefficient of penetrant 1 solvated in the composite matrix.

If both types of penetrants diffuse in two types of matrices, PMPC and PMPF, equation (49) would be obtained:

$$\frac{Sel_{cal,PMPC}}{Sel_{cal,PMPF}} = \frac{Sel_{\exp,PMPC}}{Sel_{\exp,PMPF}} \cdot \frac{\gamma_{1,PMPC}}{\gamma_{1,PMPF}} < \frac{Sel_{\exp,PMP-C}}{Sel_{\exp,PMP-F}} \tag{49}$$

From equation (49) it is seen that if the solubility of penetrant 1 in PMPF is higher than in

PMPC, the corresponding activity coefficient in PMPF will be higher.

3.3 Results and Discussions

The results and discussions are to be presented in the section.

3.3.1 Cavity size distribution

The cavity size distribution is presented in Figure 3.2.

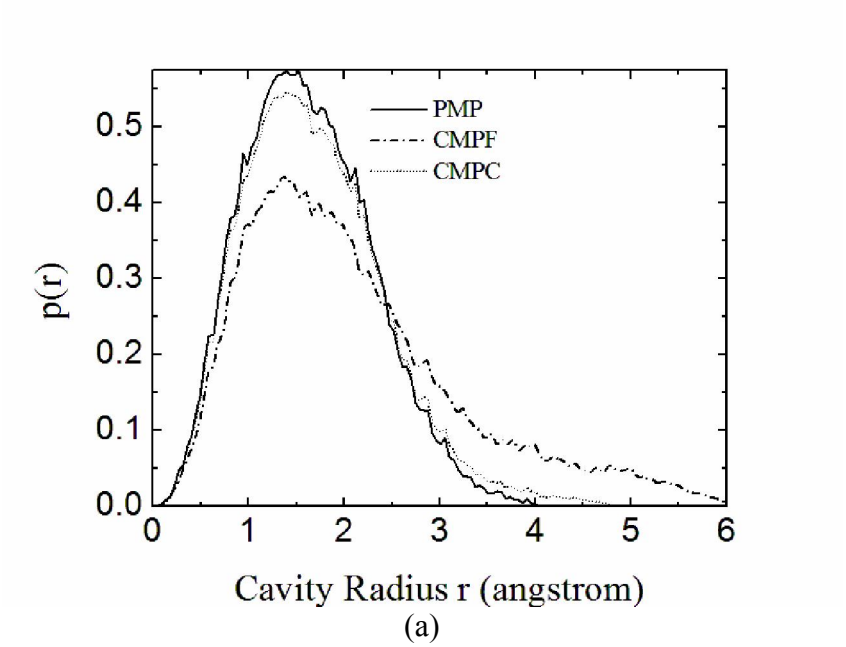

(a)

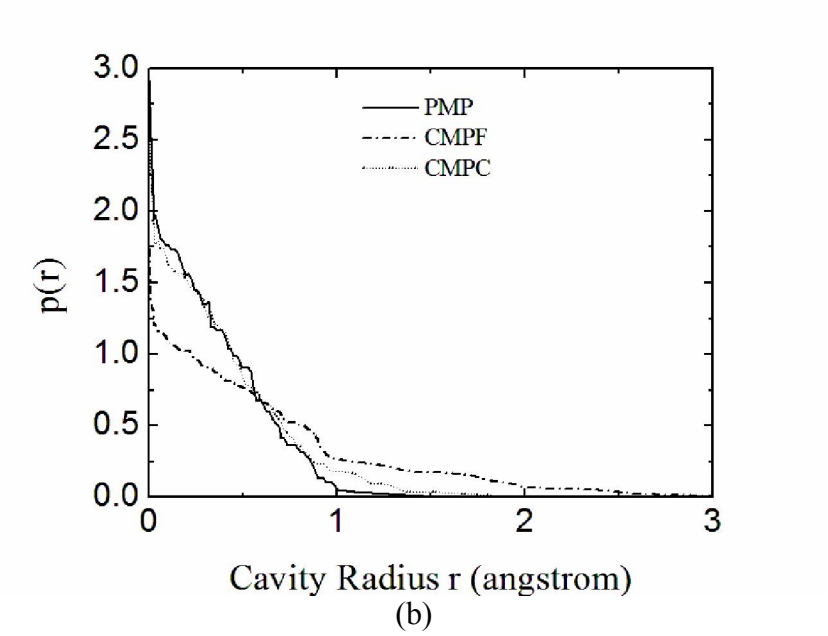

(b)

Figure 3.2. The cavity size distribution in PMP, PMPC and PMPF; p(r) is the probability of the cavity radius being r. (a) shows the cavity radius distribution when the size of the matrix units is ignored (regarded as zero); (b) shows the cavity radius distribution when the diameter of the matrix units is considered as equal to the Lennard-Jones size parameters of the corresponding units.

To get a clear picture of the real cavity size distribution in PMP and the composite, two types of cavity size distribution were evaluated according to the trajectory files. When the size of the units of the matrix is ignored, the cavity radius distribution in Figure 3.2(a) can be obtained. When the radius of the matrix units is considered as one half of the Lennard-Jones size parameters of the corresponding units, Figure 3.2(b) is obtained.

From Figure 3.2, it is observed that in the PMP and silica nanoparticle composite, the fraction of large cavities is higher than in pure PMP. Therefore, due to the existence of the silica nanoparticle, the cavity size distribution varies, which lead to higher diffusivity in the composite. Furthermore, the fraction of large cavities in the composite PMPF is higher than that in the composite PMPC. The pores in the faujasite silica nanoparticle contribute to the difference.

3.3.2 Diffusivity calculation

At different times, the distance of CH_4 to the simulation cell center in PMPC and PMPF are presented in Figure 3.3. The radius of the silica nanoparticle is 1.25nm. From Figure 3.3(a), it is seen that CH_4 only transports in an area further than 1.25nm from the cell center. That is the penetrant definitely cannot pass through the nanoparticle of the cristobalite silica. On the other hand, Figure 3.3(b) shows that in the composite PMPF, CH_4 penetrants can transports in an area closer than 1.25nm from the cell center. The penetrant can definitely pass through the faujasite silica nanoparticle.

The shape of the loci in Figure 3.3(a) and 3.3(b) is different. In Figure 3.3(a), it is seen that the transport is composed of large jumps separated by long quiescent long periods, while in Figure 3.3(b), the penetrant motion contains frequent diffusive jumps and lacks quiescent periods. Therefore, in the PMPC , the penetrant hops after long periods of localization in voids

in the PMP structure, while in the PMPF , the penetrant is no longer trapped in voids when it diffuses in the faujasite silica nanoparticle and the hypothesis of the penetrant motion as that of hopping between voids is no longer applicable.

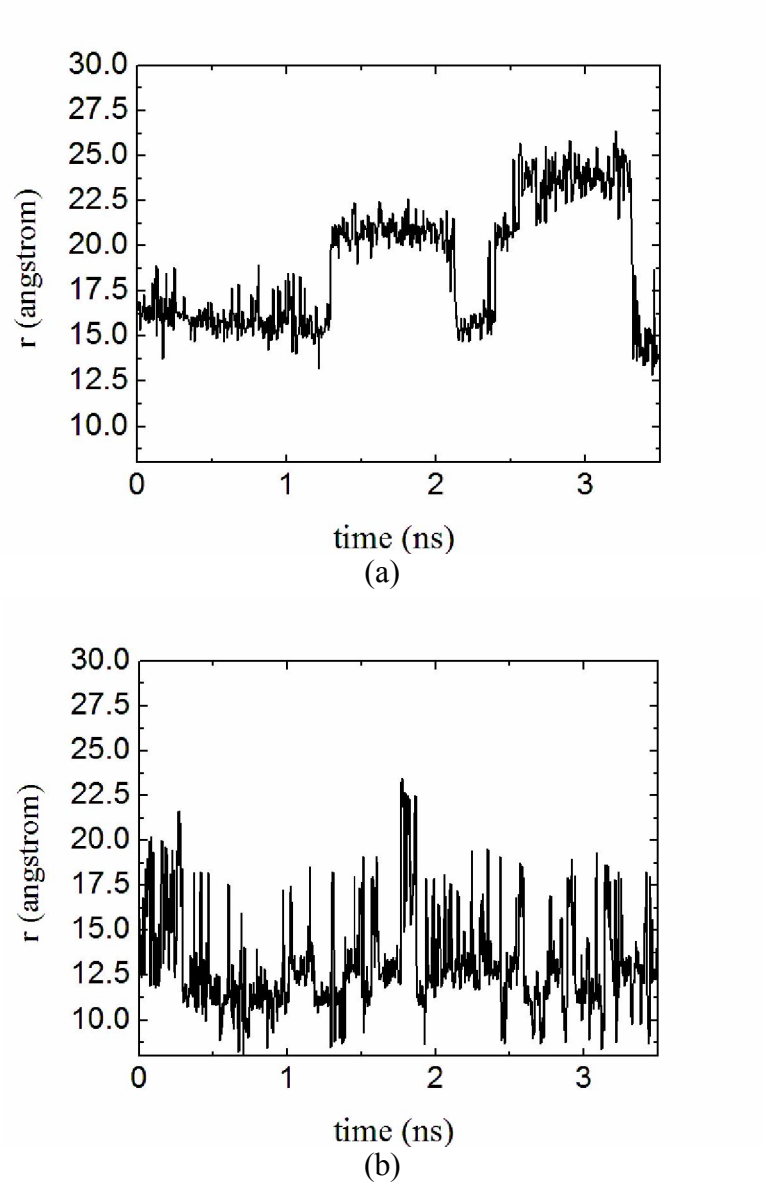

Figure 3.3: The distance, r, of CH_4 penetrant from the simulation cell center in PMPC (a) and PMPF (b) at different times.

The logarithmic plot of mean square displacement averaged over different time origin

versus time was used to determine if the transport is in the Fickian diffusive regime. Subsequently the values of the diffusivity were determined via the slope of the line obtained from a least squares fit.

Figure 3.4 shows the relationship between the mean square displacement averaged over different time origin and the time when CH_4 diffuses in PMP, PMPC and PMPF.

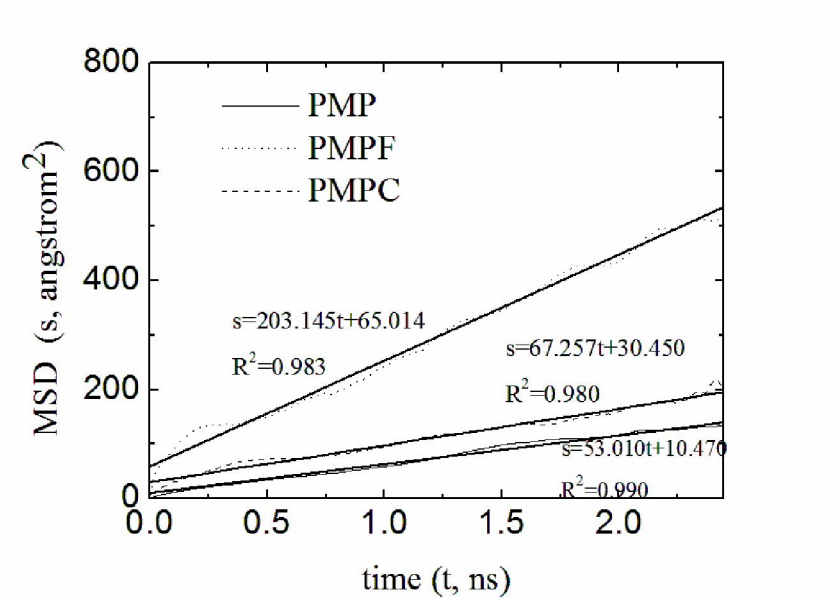

Figure 3.4: The relationship between the mean square displacement averaged over different time origin and time when CH_4 diffuses in PMP, PMPC and PMPF . R^2 is the square of correlation coefficient.

The simulation results of diffusivity of different penetrants in PMP, PMPC and PMPF are presented in Table 3.1.

Table 3.1. Diffusivity of penetrants in PMP, in PMPC and in PMPF ($D \times 10^9 m^2/s$). The data in the parenthesis is the standard deviation.

Diffusivity / Penetrants	D_{PMP}	D_{PMPC}	D_{PMPF}
H_2	47.5(16.1)	31.7(8.9)	136.1(39.2)
O_2	0.610(0.17)	4.31(1.23)	7.52(3.21)
Ar	0.166(0.07)	0.732(0.327)	1.053(0.345)
CH_4	0.092(0.05)	0.112(0.051)	0.338(0.171)
n-C_4H_{10}	0.030(0.02)	0.108(0.054)	0.115(0.063)

From Table 3.1 it is observed that from H_2, O_2, CH_4, Ar to n-C_4H_{10}, the corresponding diffusivity in PMP, PMPC, and PMPF decreases. This trend matches the changing trend of the diffusivity of these penetrants in polyethylene.

3.3.3 Computation of solubility coefficients and permeability

The solubility coefficients of CH_4 in PMP, in the PMPC and in PMPF at different time are presented in Figure 3.5.

The solubility coefficients calculation results of different penetrants in PMP and composite are listed in Table 3.2. The weight concentration of penetrants in PMP is $\frac{m_{penetrants}}{m_{penetrants} + m_{PMP}}$, while that in composite is $\frac{m_{penetrants}}{m_{penetrants} + m_{PMP} + m_{NP}}$.

Form Table 3.2 it is observed that from H_2, O_2, Ar, CH_4 to n-C_4H_{10}, the corresponding solubility coefficients decreases. This trend matches the changing trend of the solubility values of these penetrants in polyethylene [92].

Table 3.2 The calculated solubility coefficients calculation results of different penetrants in PMP and two types of composites. The data in the first parenthesis are the standard deviation; the data in the second parenthesis of each cell are weight concentration of the penetrants. The units are all 1.

Penetrant / matrix	PMP	PMPC	PMPF
H_2	0.250(0.0631)(0.0000248)	0.320(0.074)(0.0000318)	0.725 (0.120) (0.0000720)
O_2	0.269 (0.117) (0.000790)	0.381(0.134)(0.00112)	1.345 (0.245) (0.00213)
Ar	0.838 (0.216) (0.00307)	3.235(0.647)(0.0119)	12.567 (3.283) (0.0251)
CH_4	1.654 (0.323) (0.00243)	7.539(1.398)(0.0117)	65.231 (11.024) (0.0517)
n-C_4H_{10}	107.304 (24.167) (0.363)	305.376(142.566)(0.584)	6002.36(2192.75)(0.898)

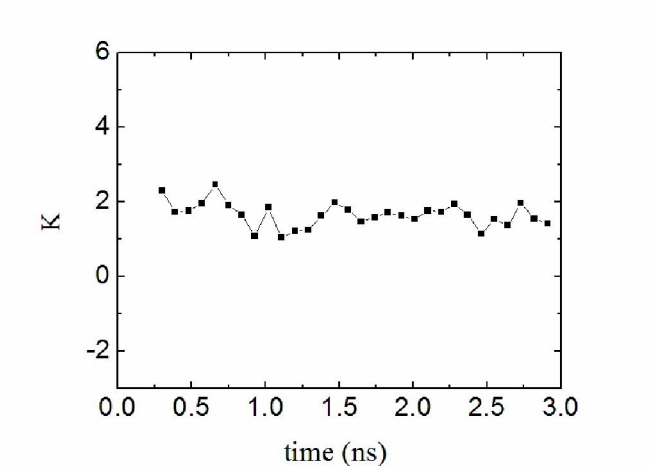

(a)

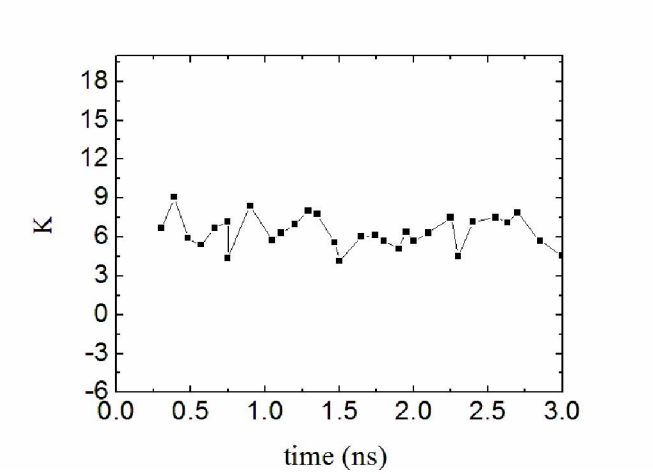

(b)

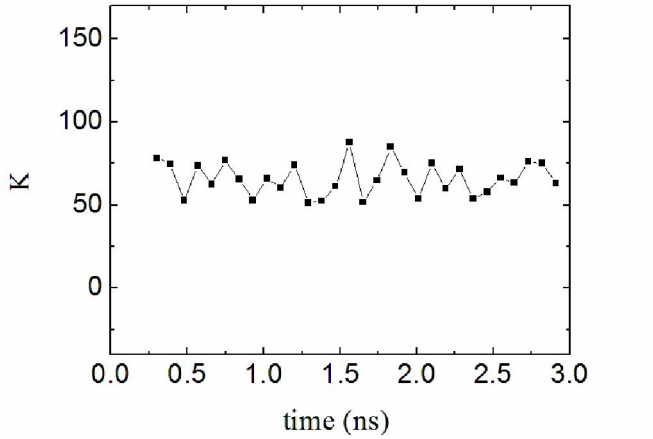

(c)

Figure 3.5. The solubility coefficients of CH_4 in PMP (a), PMPC (b) and PMPF (c) at different time

To explore the space distribution of potential difference in the simulation cell due to the penetrant insertion, 10000 successive random insertions were done in the matrix structure corresponding to 2.5ns in Figure 3.5(b) and 3.5(c). According to equation (37), the contribution of each insertion is proportional to $e^{-\Delta E/RT}$. Calculation results show that in both PMPC and PMPF, the 25 insertions with the 25 lowest potential changes account for 99.6% of the contributions of all the insertions. Figure 3.6(a) and 3.6(b) shows the values of the 25 lowest potential differences and the corresponding position of the insertions in PMPC and PMPF, respectively. The label number *i* means that the corresponding potential difference is the *i*th lowest potential differences. From Figure 3.6, it is observed that in PMPC, the positions of the 25 insertions that contribute most are further from the cell center than 1.25nm. In contrast, in PMPF, the 25 insertions that contribute most locate inside the faujasite silica nanoparticle; therefore in PMPF the nanoparticle solvates most penetrants; it is the large pores in the faujasite silica nanoparticle and the strong interaction between the penetrants and the Si and O atoms of the nanoparticle that lead to the high solubility of different penetrants.

Then with the values of diffusivity and solubility coefficients, the permeability values of different penetrants in PMP and PMP and silica nanoparticle composite were calculated and listed in Table 3.3

Table 3.3 shows that in PMP and PMPC the calculated permeability of CH_4 is closer to the experimental values than the computed permeability of n-C_4H_{10}. The solubility of n-C_4H_{10} is high in PMP compared with O_2 and CH_4. The size of n-C_4H_{10} is larger than O_2 and CH_4. The insertion of these n-C_4H_{10} molecules will cause more changes of matrices structures. The activity coefficient of n-C_4H_{10} in PMP will differ more from one than O_2 and CH_4. Therefore the calculated permeability of n-C_4H_{10} in PMP will differ more from the corresponding experimental values than O_2 and CH_4.

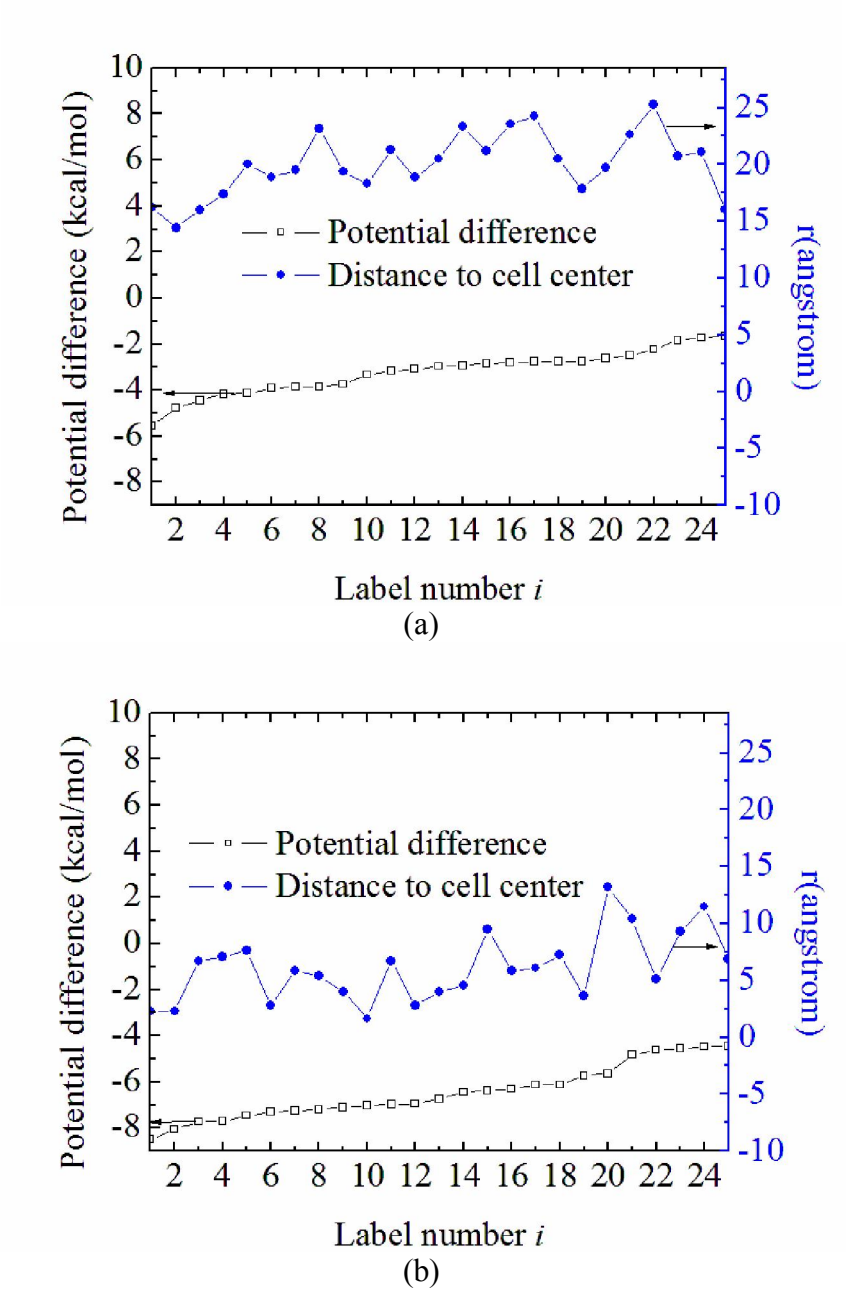

Figure 3.6. (a) and (b) shows the values of the 25 lowest potential differences and the corresponding position of the insertions in PMPC and PMPF, respectively. The label number *i* means that the corresponding potential difference is the *i*th lowest.

Table 3.3 Calculated permeability of different penetrants in PMP and composites; the date in parenthesis are the corresponding experimental results.

penetrants / matrix	PMP		PMPC		PMPF
	$P\,(10^3 barrer)$	γ	$P(10^3 barrer)$	γ	$P(10^3 barrer)$
H_2	15.623	-	13.349	-	129.853
O_2	0.216 (0.185) [103,108]	1.167	2.161	-	13.311
Ar	0.183	-	3.116	-	17.415
CH_4	0.203(0.191) [109]	1.068	1.113(0.873) [109]	1.275	29.015
n-C_4H_{10}	4.236 (2.735) [109]	1.549	43.403(22.357) [109]	1.942	908.397

From Table 3.3, it is observed that the two types of composites both have higher permeability than PMP for the same penetrants. Especially for n-C_4H_{10} the insertion of silica nanoparticle in PMP significantly increases permeability. The selectivity of CH_4 over O_2 does not differ much from one in both PMP and composites, as the molecule sizes and VDW interaction of CH_4 with matrix atoms are close to O_2. The selectivity of n-C_4H_{10} over CH_4 increases from 20 to 31 due to the insertion of faujasite silica nanoparticle, and to 38 because of the insertion of cristobalite silica nanoparticle. The ratio of the computed value of selectivity of n-C_4H_{10} over CH_4 in PMPC to that in PMPF is therefore 38/31.

When two types of penetrants, n-C_4H_{10} (1) and CH_4 (2), are transported in matrices, the solubility of n-C_4H_{10} in PMPF is significant higher than in PMPC and the corresponding activity coefficient will be higher. According to equation (49), the ratio of the experimental value of selectivity of n-C_4H_{10} over CH_4 in PMPC to that in PMPF would be higher than 38/31. The PMP and nanoparticle of cristobalite composite has better performance and is therefore widely employed to separate the mixture of n-C_4H_{10} with CH_4 in industry [103, 109].

3.4 Conclusion

In industry, the separation of gas mixtures is of considerable siginificance. The PMP and silica nanoparticle composite is used to separate C_4H_{10} (n-butane) from mixtures of C_4H_{10} and CH_4, H_2, etc. Silica has different crystalline forms. The transport properties of penetrants in the composite PMP and nanoparticles of these two forms of silica are different. It is essential to explore the real reasons that lead to the difference to aid the design of membranes made of PMP and silica nanoparticle composites. The molecular dynamics method was employed in the work to explore the transport of different penetrants, including H_2, O_2, CH_4, Ar and C_4H_{10} in PMP and the composites of PMP and two forms of silica nanoparticles, the cristobalite form and the faujasite form. The structure of the PMPC and PMPF was established and relaxed. With the structure, the cavity size distribution was analyzed and it is observed that PMP and silica nanoparticle composite has more large cavities than pure PMP, while PMPF has more large cavities than PMPC. The diffusivity of different penetrants was determined through least square fit of the data of mean square displacement at different times in Fickian diffusive regime. The results show that from H_2, O_2, CH_4, Ar to n-C_4H_{10}, the corresponding diffusivity in PMP decreases. This trend matches the changing trend of the diffusivity of these penetrants in polyethylene. The solubility coefficients and the permeability of different penetrants in PMP and the composite were calculated.

The calculated results show that the two types of composites both have high permeability compared with PMP for the same penetrants and PMPF has higher permeability than PMPC for the same penetrants. The selectivity of n-C_4H_{10} over CH_4 increases from 20 to 31 due to the insertion of faujasite silica nanoparticle, and to 38 because of the insertion of cristobalite silica nanoparticle. The ratio of the real selectivity of n-C_4H_{10} over CH_4 in PMPC to that in PMPF is higher than 38/31. PMPC has better performance than PMPF and is widely employed to

separate the mixture of n-C_4H_{10} with other gas molecules, like CH_4, in industry.

Chapter 4

Simulating penetrants transport in composite poly (4-methyl-2-pentyne) and TiO_2 nanoparticles through molecular dynamics method

4.1 Introduction

Currently, there is a lot of research in membranes, penetrant transport and molecular dynamics simulation [110-144]. In industry, the membranes made of composite poly (4-methyl-2-pentyne) and TiO_2 nanoparticles are employed to treat alkane gas mixtures. It is necessary to research the penetrants transport in the PMP and TiO_2 nanoparticles composite. However, no researchers have explored the penetrants transport in the PMP and TiO_2 nanoparticles composite employing molecular dynamics simulation method. The VDW parameters for Ti was fitted according to the Buckingham potential with specific *A*, *B*, *C* values obtained from literature. The structure of the PMP and TiO_2 composite was established and relaxed firstly. Then the diffusivity, solubility, and permeability of different penetrants in PMP and TiO_2 composite were determined and compared with PMP and silica composite. In this chapter, the research results are presented.

4.2 Computational Method

Researchers [146-149] tend to use VDW potential for Ti atoms in the form of Buckingham potential:

$$U(r_{bc}) = A\exp(-\frac{r_{bc}}{B}) - \frac{C}{r_{bc}^6} \tag{50}$$

The most widely acceptable Buckingham potential for Ti atoms is the one Matsui and Akoagi [146, 147, 150, 151] developed. The values of specific *A*, *B*, *C* are listed in the following table.

Table 4.1 The values of specific *A*, *B*, *C* of the Buckingham potential

A (kcal mol^{-1})	B (angstrom)	C(kcal $angstrom^6$ mol^{-1})
717700	0.154	121.0

However, to do MD simulations, the potential function in the form of Lennard-Jones potential is needed.

Lennard-Jones potential:

$$U(r_{bc}) = 4\varepsilon[(\frac{\sigma}{r_{bc}})^{12} - (\frac{\sigma}{r_{bc}})^{6}] \tag{22}$$

That is the ε and σ parameters must be fitted according to the Buckingham potential with specific *A*, *B*, *C* values. The least square fit was employed and the result is:

$\sigma = 3.024$ angstrom $\quad \varepsilon = 0.745$ kcal/mol

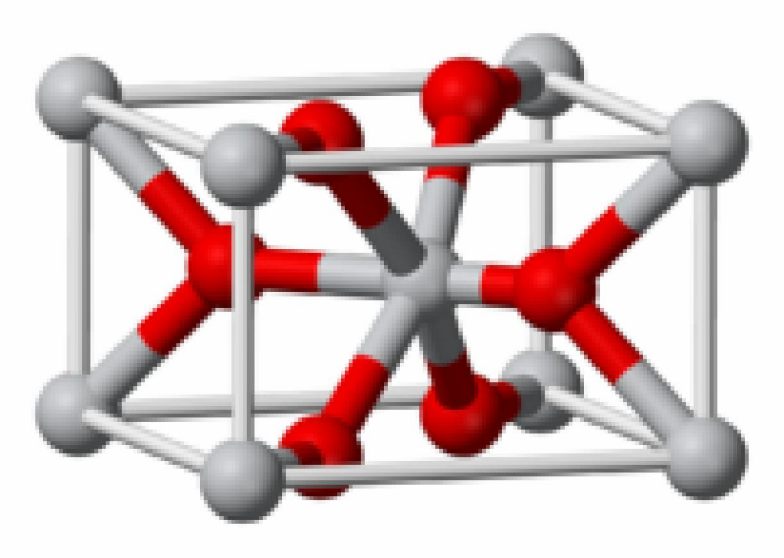

Figure 4.1: Unit cell of TiO_2 nanoparticle

Figure 4.1 shows the structure unit of the TiO_2 nanoparticle, where the red balls represent Ti atoms and the white balls stand for O atoms. Based on the unit cell, the structure of TiO_2 nanoparticle with diameter of 2.5 nm was created. Replace the silica nanoparticle in the simulations done before with the TiO_2 nanoparticle, the system of the PMP and TiO_2 nanoparticle composite can be established. The system was relax completely and then MD simulation was done to simulate penetrants transport in the composite system based on the relax system. The same methods as described in Chapter 2 and Chapter 3 [152, 153] were employed to determine diffusivity, solubility, and permeability of different penetrants in the composite. Finally, the simulation results were compared with the results of PMP and silica nanoparticle composite.

4.3 Diffusivity calculation

At different times, the distance of CH_4 to the simulation cell center in PMPT and PMPF are presented in Figure 4.2.

The radius of the TiO_2 nanoparticle is 1.25nm. From Figure 4.2(a), it is seen that CH_4 only

transports in an area further than 1.25nm from the cell center. That is the penetrant definitely cannot pass through the nanoparticle of the TiO_2, as in cristobalite silica.

In Figure 4.2(a), it is seen that the transport is composed of large jumps separated by long quiescent long periods, while in Figure 4.2(b), the penetrant motion contains frequent diffusive jumps and lacks quiescent periods. Therefore, in the PMPT and PMPC, the penetrant hops after long periods of localization in voids in the PMP structure, while in the PMPF the penetrant is no longer trapped in voids when it diffuses in the faujasite silica nanoparticle and the hypothesis of the penetrant motion as that of hopping between voids is no longer applicable.

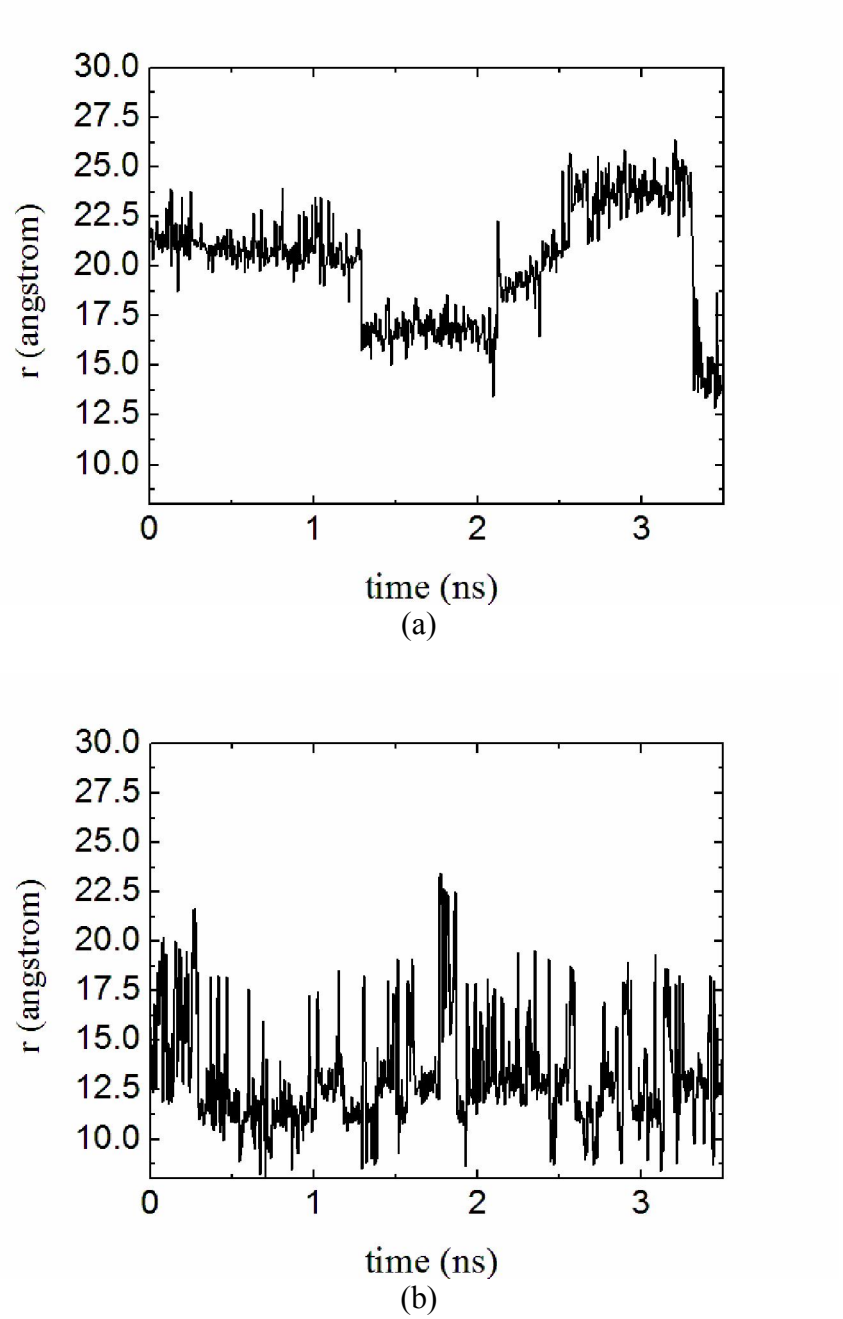

Figure 4.2: The distance, r, of CH_4 penetrant from the simulation cell center in PMPT (a) and PMPF (b) at different times.

The logarithmic plot of mean square displacement averaged over different time origin

versus time was used to determine if the transport is in the Fickian diffusive regime. Subsequently the values of the diffusivity were determined via the slope of the line obtained from a least squares fit.

The simulation results of diffusivity of different penetrants in PMP, PMPC, and PMPF are presented in Table 4.2.

Table 4.2: Diffusivity of penetrants in PMP, in PMPC and in PMPT ($D \times 10^9 m^2/s$). The data in the parenthesis is the standard deviation.

Diffusivity / Penetrants	D_{PMP}	D_{PMPC}	D_{PMPT}
H_2	47.5(16.1)	31.7(8.9)	37.5(15.2)
O_2	0.610(0.17)	4.31(1.23)	4.75(1.24)
Ar	0.166(0.07)	0.732(0.327)	0.842(0.247)
CH_4	0.092(0.05)	0.112(0.051)	0.123(0.073)
n-C_4H_{10}	0.030(0.02)	0.108(0.054)	0.132(0.061)

From Table 4.2 it is observed that from H_2, O_2, CH_4, Ar to n-C_4H_{10}, the corresponding diffusivity in PMP, PMPC and PMPT decreases. This trend matches the changing trend of the diffusivity of these penetrants in polyethylene.

4.4 Computation of solubility coefficients and permeability

The solubility coefficients of CH_4 in PMP, in the PMPC and in PMPT at different time are presented in Figure 4.3.

The solubility coefficients calculation results of different penetrants in PMP and composite are listed in Table 4.3. The weight concentration of penetrants in PMP is $\frac{m_{penetrants}}{m_{penetrants} + m_{PMP}}$, while that in composite is $\frac{m_{penetrants}}{m_{penetrants} + m_{PMP} + m_{NP}}$.

Form Table 4.3 is observed that from H_2, O_2, Ar, CH_4 to n-C_4H_{10}, the corresponding solubility coefficients decreases. This trend matches the changing trend of the solubility values of these penetrants in polyethylene [92].

Table 4.3:The calculated solubility coefficients calculation results of different penetrants in PMP and two types of composites. The data in the first parenthesis are the standard deviation; the data in the second parenthesis of each cell are weight concentration of the penetrants. The units are all 1.

Penetrant / matrix	PMP	PMPC	PMPT
H_2	0.250(0.0631)(0.0000248)	0.320(0.074)(0.0000318)	0.415 (0.120) 0.0000720)
O_2	0.269 (0.117) (0.000790)	0.381(0.134)(0.00112)	0.546 (0.245) (0.00213)
Ar	0.838 (0.216) (0.00307)	3.235(0.647)(0.0119)	4.732 (3.283) (0.0251)
CH_4	1.654 (0.323) (0.00243)	7.539(1.398)(0.0117)	8.673 (11.024) (0.0517)
n-C_4H_{10}	107.304 (24.167) (0.363)	305.376(142.566)(0.584)	423.56(2192.75)(0.898)

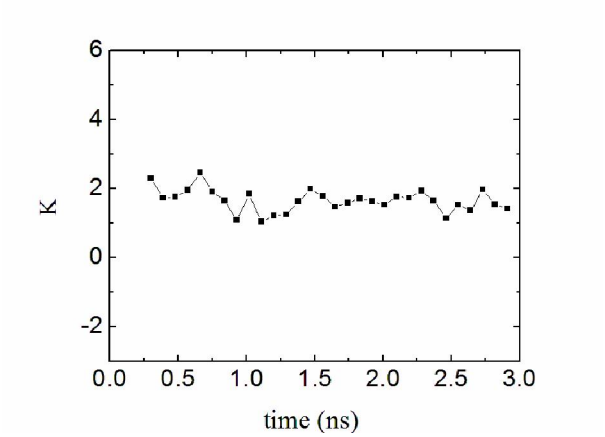

(a)

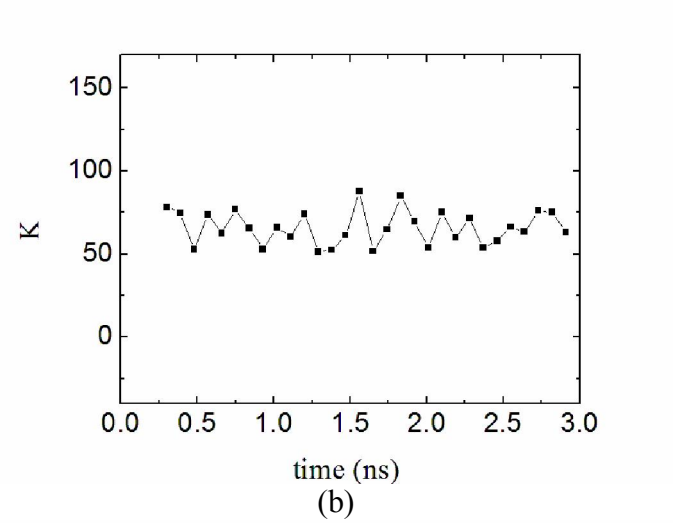

(b)

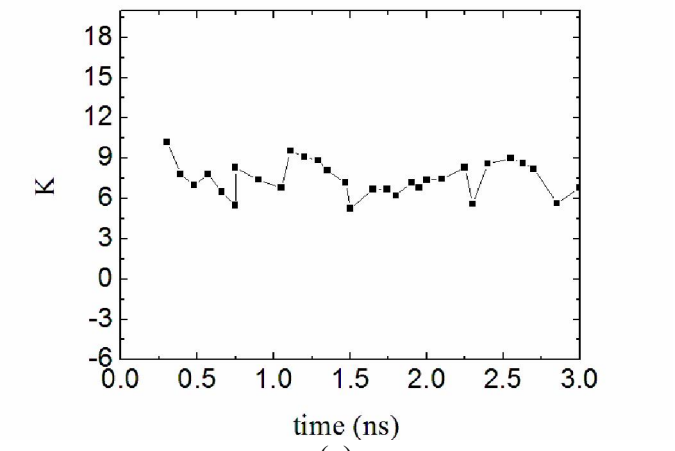

(c)

Figure 4.3: The solubility coefficients of CH_4 in PMP (a), PMPF (b) and PMPT (c) at different time

To explore the space distribution of potential difference in the simulation cell due to the penetrant insertion, 10000 successive random insertions were done in the matrix structure corresponding to 2.5ns in Figure 4.3(b) and 4.3(c). According to equation (49), the contribution of each insertion is proportional to $e^{-\Delta E / RT}$. Calculation results show that in both PMPT and PMPF, the 25 insertions with the 25 lowest potential changes account for 99.6% of the contributions of all the insertions. Figure 4.4(a) and 4.4(b) shows the values of the 25 lowest potential differences and the corresponding position of the insertions in PMPT and PMPF, respectively. The label number *i* means that the corresponding potential difference is the *i*th lowest potential differences. From Figure 4.4, it is observed that in PMPT, the positions of the 25 insertions that contribute most are further from the cell center than 1.25nm. In contrast, in PMPF, the 25 insertions that contribute most locate inside the faujasite silica nanoparticle; therefore in PMPF the nanoparticle solvates most penetrants; it is the large pores in the faujasite silica nanoparticle and the strong interaction between the penetrants and the Si and O atoms of the nanoparticle that lead to the high solubility of different penetrants.

Then with the values of diffusivity and solubility coefficients, the permeability values of different penetrants in PMP and composites were calculated and listed in Table 4.4.

Table 4.4 shows that in PMP and PMPC the calculated permeability of CH_4 is closer to the experimental values than the computed permeability of n-C_4H_{10}. The solubility of n-C_4H_{10} is high in PMP compared with O_2 and CH_4. The size of n-C_4H_{10} is larger than O_2 and CH_4. The insertion of these n-C_4H_{10} molecules will cause more changes of matrices structures. The activity coefficient of n-C_4H_{10} in PMP will differ more from one than O_2 and CH_4. Therefore the calculated permeability of n-C_4H_{10} in PMP will differ more from the corresponding experimental values than O_2 and CH_4.

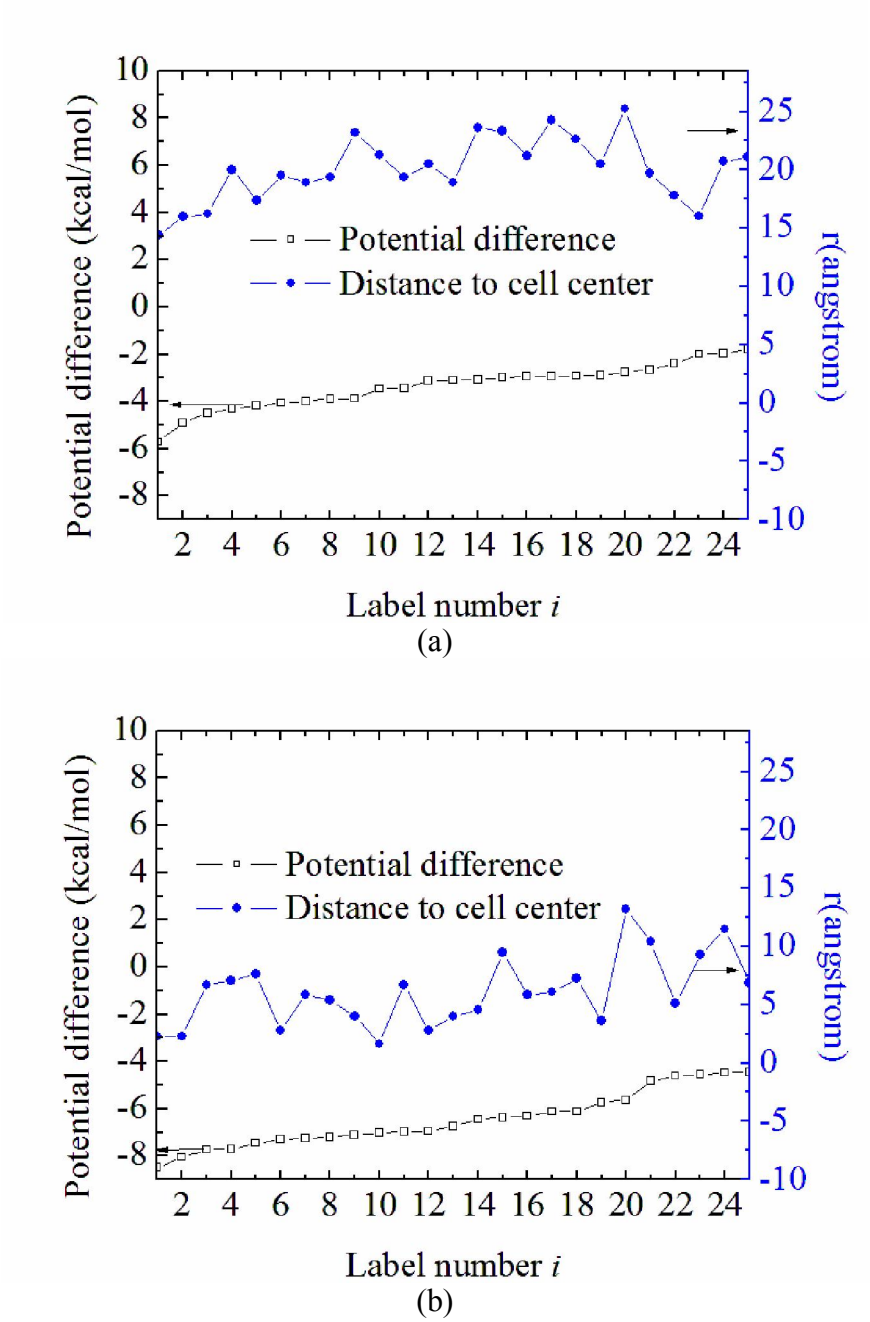

Figure 4.4: (a) and (b) shows the values of the 25 lowest potential differences and the corresponding position of the insertions in PMPT and PMPF, respectively. The label number *i* means that the corresponding potential difference is the *i*th lowest.

Table 4.4: Calculated permeability of different penetrants in PMP and composites; the date in parenthesis are the corresponding experimental results.

Penetrants / Matrix	PMP		PMPC		PMPT
	$P\,(10^3 barrer)$	γ	$P(10^3 barrer)$	γ	$P(10^3 barrer)$
H_2	15.623	-	13.349	-	20.479
O_2	0.216 (0.185)	1.167	2.161	-	3.413
Ar	0.183	-	3.116	-	5.243
CH_4	0.203(0.191)	1.068	1.113(0.873)	1.275	1.403
n-C_4H_{10}	4.236 (2.735)	1.549	43.403(22.357)	1.942	73.567

From Table 4.4, it is observed that the two types of composites both have higher permeability than PMP for the same penetrants. Especially for n-C_4H_{10} the insertion of silica nanoparticle in PMP significantly increases permeability. The selectivity of CH_4 over O_2 does not differ much from one in both PMP and composites, as the molecule sizes and VDW interaction of CH_4 with matrix atoms are close to O_2. The selectivity of n-C_4H_{10} over CH_4 increases from 20 to 38 due to the insertion of cristobalite silica nanoparticle, and to 52 because of the insertion of nanoparticle of TiO_2. The ratio of the computed value of selectivity of n-C_4H_{10} over CH_4 in PMPT to that in PMPC is therefore 52/38.

4.5 Conclusion

In industry, the separation of gas mixtures is of considerable significant. The PMP and TiO_2 nanoparticle composite (PMPT) is used to separate C_4H_{10} (n-butane) from mixtures of C_4H_{10} and CH_4, H_2, etc. It is essential to explore the penetrants transport in PMPT from molecular level. Molecular dynamics method was employed in the work to explore the transport of different penetrants, including H_2, O_2, CH_4, Ar and C_4H_{10} in PMPT. The VDW parameters needed in the molecular dynamics simulation were fitted successfully. The structure of the PMPT was established and relaxed. The diffusivity of different penetrants was determined through least square fit of the data of mean square displacement at different times in Fickian

diffusive regime. The results show that from H_2, O_2, CH_4, Ar to n-C_4H_{10}, the corresponding diffusivity in PMPT decreases. This trend matches the changing trend of the diffusivity of these penetrants in polyethylene. The solubility coefficients and the permeability of different penetrants in PMPT were calculated.

The calculated results show that PMPT has high permeability compared with PMP for the same penetrants. The selectivity of n-C_4H_{10} over CH_4 increases from 20 to 38 due to the insertion of cristobalite silica nanoparticle, and to 52 because of the insertion of nanoparticle of TiO_2. The ratio of the computed value of selectivity of n-C_4H_{10} over CH_4 in PMPT to that in PMPC is therefore 52/38.

Chapter 5

Summary

The penetrants transport in composite PMP and different types of nanoparticles has been researched thoroughly employing molecular dynamics simulation method:

Firstly, the penetrants transport in PMP and amorphous silica nanoparticle composite was explored. The structure of the PMP and silica nanoparticle composite was established. With the structure, the cavity size distribution was analyzed and it is observed that in the PMP and silica nanoparticle composite, larger cavities exist than in pure PMP, which lead to the increase in diffusivity in the composite than in pure PMP. The diffusivity of different penetrants, including H_2, O_2, Ar, CH_4 and n-C_4H_{10} was determined through least square fit of the data of mean square displacement at different time in Fickian diffusive regime. Based on the resistance concept in heat and mass transport, I developed an equation to correlate the diffusivity of the same penetrants in different materials. The equation can be employed to predict diffusivity in the composite with the diffusivity values in PMP and zeolite. The solubility coefficients and the permeability of different penetrants in PMP and the composite were calculated. The distribution of potential difference due to the penetrant insertion was explored in detail. The results show that the interaction between Si and O atoms of the nanoparticle and penetrants causes the higher solubility in composite, not because of the shape change of PMP chains. Because the solubility of n-C_4H_{10} is high in PMP compared with O_2 and CH_4, the activity

coefficient of O_2 and CH_4 will be closer to one than that of n-C_4H_{10} and the calculated permeability of O_2 and CH_4 is closer to the experimental values than the computed permeability of n-C_4H_{10}. Finally, the influence of weight concentration of nanoparticles on penetrants transport was explored.

Secondly, molecular dynamics simulation was done to compare the penetrants transport in composite poly (4-methyl-2-pentyne) and two forms of silica. The structure of the PMPC and PMPF was established and relaxed. With the structure, the cavity size distribution was researched and it is observed that PMP and silica nanoparticle composite has more large cavities than pure PMP, while PMPF has more large cavities than PMPC. The diffusivity of different penetrants was determined through least square fit of displacement at different times in the Fickian diffusive regime. The results show that from H_2, O_2, CH_4, Ar to n-C_4H_{10}, the corresponding diffusivity in PMP decreases. This trend matches the changing trend of the diffusivity of these penetrants in polyethylene. The solubility coefficients and the permeability of different penetrants in PMP and the composite were calculated. The calculated results show that the two types of composites both have high permeability compared with PMP for the same penetrants and PMPF has higher permeability than PMPC for the same penetrants. The selectivity of n-C_4H_{10} over CH_4 increases from 20 to 31 due to the insertion of faujasite silica nanoparticle, and to 38 because of the insertion of cristobalite silica nanoparticle. The ratio of the real selectivity of n-C_4H_{10} over CH_4 in PMPC to that in PMPF is higher than 38/31, anyway higher than 1. PMPC is widely employed to separate the mixture of n-C_4H_{10} with other gas molecules, like CH_4 , in industry.

Thirdly, the penetrants transport was simulated in composite poly (4-methyl-2-pentyne) and TiO_2 nanoparticles through molecular dynamics method. The structure of the PMPT was successfully established and relaxed. The diffusivity of different penetrants was determined according to the least square fit of the data of mean square displacement at different times in

Fickian diffusive regime. From the results it is shown that from H_2, O_2, CH_4, Ar to n-C_4H_{10}, the corresponding diffusivity in PMPT decreases. This trend matches the changing trend of the diffusivity of these penetrants in polyethylene. The solubility coefficients and the permeability of different penetrants in PMPT were calculated. The calculated results show that PMPT has high permeability compared with PMP for the same penetrants. The selectivity of n-C_4H_{10} over CH_4 increases from 20 to 38 because of the insertion of cristobalite silica nanoparticle, and to 52 due to the insertion of nanoparticle of TiO_2. So the ratio of the computed value of selectivity of n-C_4H_{10} over CH_4 in PMPT to that in PMPC is 52/38, higher than 1.

Currently, the penetrant transport in the PMP composite has been research thoroughly. In the future, the relationship between cavity radius distribution and free volume ratio will be researched. The composite containing carbon nanotubes will also be explored. It is now a very popular research realm.

Nomenclature

C_0 = Ideal gas concentration at standard condition, kmol/m^3

C = Concentration of penetrants, kmol/m^3

D = Diffusivity, m^2/s

ΔE = Potential energy difference, kcal/mol

H = Henry's constant

K = Solubility coefficient

MSD = Mean square displacement (nm^2 or angstrom^2)

N = Number of insertions

$p(r)$ = The probability density of the cavity radius being r

P = Permeability, barrer

r = Displacement, nm or angstrom

$\underline{R}$ = Displacement (vector), nm or angstrom

R = Universal gas constant, 8.314J/(mol·K)

S = Solubility, kmol/m^3

t = Time, fs, ps or ns

T = Temperature, K

x = Mole fraction

ε = Energy parameter of Lennard-Jones equation (lowest energy, kcal/mol).

γ = Activity coefficient (modification factor) of penetrants in matrices

σ = Size parameter of Lennard-Jones equation (where the potential energy equals zero, nm)

Subscripts

m = Matrices

Cal = Calculated values

Exp = Experimental values

$PMPC$ = The PMP and cristobalite silica nanoparticle composite

$PMPF$ = The PMP and faujasite silica nanoparticle composite

PMP = Poly (4-methyl-2-pentyne)

References

[1] EPA Guideline Series, Control of Volatile Compounds from Manufacture of High Density Polyethylene, Polypropylene, and Polystyrene Resins PB 84 134600, November 1984

[2] J. S. Smith, D. Bedrova, G. D. Smith, A molecular dynamics simulation study of nanoparticle interactions in a model polymer-nanoparticle composite. Composites Sci. Tech. 2003, 63, 1599–1605.

[3] B. Flaconnèche, J. Martin, M. H. Klopffer, Transport Properties of Gases in Polymers: Experimental Methods, Oil Gas Sci. Technol. 56 (3), 2001, 245-259

[4] S. A. Stern, Polymers for Gas Separations: the next dacade. J. Memb. Sci., 94, 1994, 1-65

[5] J. Klein, B. J. Briscoe, Diffusion of long molecules through solid polyethylene. II. Measurement and results. J. Polym. Sci., Polym. Phys. Ed. 1977, 15, 2065-2074.

[6] A. Rawls, Diffusion of an erucamide slip additive in linear low-density polyethylene film. M.S., Clemson University, 1997.

[7] N. E. Schlotter, P. Y. Furlan, A review of small molecule diffusion in polyolefins polymer

1992, 33, 3323-3342.

[8] V. Stannett, The transport of gases in synthetic polymeric membranes-an historic perspective. J. Membr. Sci. 1978, 3, 97-115.

[9] J. Crank, Methods of measurement. In Diffusion in Polymers; J. Crank and G. S. Park, Eds.; Academic Press: New York, 1968

[10] H. L. Frisch, The time lag in diffusion. J. Phys. Chem. 1957, 61, 93-95.

[11] N. Vahdat, V. D. Sullivan, Estimation of permeation rate of chemical through elastometric materials. J. Appl. Polym. Sci. 2000, 79, 1265-1272.

[12] R. M. Felder, G. S. Huvard, Permeation, diffusion, and sorption of gases and vapors. In Methods of Experimental Physics: Polymers; R. A. Fava, Ed.; Academic Press: New York, 1980; pp 315-377.

[13] T. V. M. Ndoro, E. Voyiatzis, A. Ghanbari, D. N. Theodorou, M. C. Bohm, F. Muller-Plathe, Interface of Grafted and Ungrafted Silica Nanoparticles with a Polystyrene Matrix: Atomistic Molecular Dynamics Simulations. Macromolecules 2011, 44(7), 2316-2327

[14] G. Milano, G. Santangelo, F. Ragone, L. Cavallo, A. Di Matteo, Gold Nanoparticle/Polymer Interfaces: All Atom Structures from Molecular Dynamics Simulations, J. Phys. Chem. C 2011, 115(31), 15154-15163

[15] B. B. Hong, A. Z. Panagiotopoulos, Molecular Dynamics Simulations of Silica Nanoparticles Grafted with Poly(ethylene oxide) Oligomer Chains, J. Phys. Chem. B 2012, 116(8), 2385-2395

[16] J. R. Spaeth, I. G. Kevrekidis, A. Z. Panagiotopoulos, Dissipative particle dynamics simulations of polymer-protected nanoparticle self-assembly. J. Chem. Phys. 2011, 135 (18), 184903-184908

[17] V. F. Lo, L. Yelash, S. A. Egorov, K. Binder, Interactions between polymer brush-coated spherical nanoparticles: the good solvent case. J. Chem. Phys. 2011, 135 (21), 214902-214910

[18] S. A. Egorov, Anomalous nanoparticle diffusion in polymer solutions and melts: a mode-coupling theory study. J. Chem. Phys. 2011, 134, 084903-084908

[19] D. E. Spearot, A. Sudibjo, V. Ullal, A. Huang, Molecular Dynamics Simulations of Diffusion of O2 and N2 Penetrants in Polydimethylsiloxane-Based Nanocomposites, J. Eng. Mater. Technol. 2012, 134(2), 021013-021020

[20] J. Liu, Y. Gao, D. Cao, L. Zhang, Z. Guo, Nanoparticle dispersion and aggregation in polymer nanocomposites: Insights from molecular dynamics simulation, Langmuir, 2011, 27(12), 7926-7933

[21] M. E. Selvan, Q. He, E. M. Calvo-Munoz, D. J. Keffer, Molecular dynamic simulations of the effect on the hydration of nafion in the presence of a platinum nanoparticle, J. Phys.

Chem. C, 2012, 116 (23), 12890-12899.

[22] Z. Wang, P. Wang, C. Hu, Investigation in influence of types of polypropylene material on diffusion by using molecular dynamics simulation. Packag Technol Sci 2012, 25(6), 329-339

[23] W. Shi, C. Ding, J. Yan, X. Han, Z. Lv, W. Lei, M. Xia, F. Wang, Molecular dynamics simulation for interaction of PESA and acrylic copolymers with calcite crystal surfaces. Desalination 2012, 291, 8-14

[24] T. Asakura, J. Yao, M. Yang, Z. Zhu, H. Hirose, Structure of the spinning apparatus of a wild silkworm Samia cynthia ricini and molecular dynamics calculation on the structural change of the silk fibroin. Polymer 2007, 48, 2064-2070

[25] W. Brostow, G. Broza, T. Datashvili, H. E. Hagg Lobland, A. Kopyniecka, Poly(butyl terephthalate) / oxytetramethylene + oxidized carbon nanotubes hybrids: Mechanical and tribological behavior. J. Mater. Res. 2012, 27, 1815-1823

[26] G. Vochita, D. Creanga, E.-l. Focanici-ciurlica, Magnetic Nanoparticle Genetic Impact on Root Tip Cells of Sunflower Seedlings. Water Air Soil Pollut. 2012, 223, 2541-2549

[27] D. Lavie, I. Drori, Collaborating for Knowledge Creation and Application: The Case of Nanotechnology Research Programs. Organ Sci. 2012, 23(3), 704-724

[28] T. Kairn, P. J. Daivis, I. Ivanov, S. N. Bhattacharya, Molecular-dynamics simulation of

model polymer nanocomposite rheology and comparison with experiment. J. Chem. Phys. 2005, 123, 194905-194911.

[29] J. W. Liu, M. E. Mackay, P. M. Duxbury, Molecular Dynamics Simulation of Intramolecular Cross-Linking of BCB/Styrene Copolymers. Macromolecules, 2009, 42, 8534-8542.

[30] E. Soolo, J. Karo, H. Kasemaegi, M. Kruusmaa, A. Aabloo, Application of the Monte Carlo method for creation of initial models of EAP molecules for molecular dynamics simulation. Proc. SPIE-Int. Soc. Opt. Eng. 2006, 6168-6179

[31] A. Adnan, C. T. Sun, H. Mahfuz, A molecular dynamics simulation study to investigate the effect of filler size on elastic properties of polymer nanocomposites. Compos. Sci. Technol. 2007, 67, 348-356.

[32] K. Hynstova, J. Jancar, J. Zidek, Molecular dynamics simulation of single chain in the vicinity of nanoparticle. Key Eng. Mater. 2007, 334-335, 373-376.

[33] Jan H. D. Boshoff, Raul F. Lobo, Norman J. Wagner， Influence of Polymer Motion, Topology and Simulation Size on Penetrant Diffusion in Amorphous, Glassy Polymers: Diffusion of Helium in Polypropylene, Macromolecules, 2001, 34, 6107-6116

[34] S. G. Charati, S. A. Stern, Diffusion of Gases in Silicone Polymers: Molecular Dynamics Simulations， Macromolecules 1998, 31, 1998, 5529-5535

[35] Y. Tamai, H. Tanaka, K. Nakanishi, Molecular Simulation of Permeation of Small Penetrants through Membranes. 1. Diffusion Coefficients. Macromolecules, 1994, 27, 4498-4508.

[36] F. Müller-Plathe, S. C. Rogers, W. F. van Gunsteren, Computational evidence for anomalous diffusion of small molecules in amorphous polymers, Chem. Phys. Lett. 1992, 199, 237.

[37] R. H. Gee, R. H. Boyd, Small penetrant diffusion in polybutadiene: a molecular dynamics simulation study, Polymer, 36 (7), 1995, 1435-1440

[38] G.E. Karlsson, U.W. Gedde, M.S. Hedenqvist, Molecular dynamics simulation of oxygen diffusion in dry and water-containing poly(vinyl alcohol), Polymer 45 (2004) 3893–3900

[39] D. Pavel,R. Shanks, Molecular dynamics simulation of diffusion of O2 and CO2 in blends of amorphous poly(ethylene terephthalate) and related polyesters, Polymer, 46(16), 2005, 6135-6147

[40] S. El Amrani and M. Kolb, Molecular dynamics simulations in zeolites: From deterministic to random motion, J. Chem. Phys. 98, 1993, 1509-1513

[41] P. Pandey, R. S. Chauhan, Membranes for gas separation, Prog. Polym. Sci. , 2001, 20, 853-83

[42] M. B. Rao, S. Sircar, Nanoporous carbon membranes for separation of gas mixtures by

selective surface flow, J. Membrane Sci.,1993, 85, 253-264

[43] V. T. Stannett, W. J. Koros, D. R. Paul, H. K. Lonsdale, R. W. Baker, Recent Advances in Membrane Science and Technology. Adv. Polym. Sci. 1979, 32, 69-121.

[44] R. W. Baker, Membrane technology, Kirk Othmer encyclopedia of chemical technology, vol.16 , Singapore: Wiley, 1995, 178-186

[45] J. S. Vrentas, J. L. Duda, Diffusion in Polymer-Solvent Systems. I. Reexamination of the Free Volume Theory. J. Polym. Sei.: Poly. Phys. Ed. 1977a, 15,403-416.

[46] R. E. Desting, A. K. Fritzcsche, Polymeric gas separation membranes, New York: Wiley, 1993, 64-70

[47] J. G. Wijmans, R. W. Baker The solution-diffusion model: a review, J. Membrane Sci., 1995, 107, 1-21

[48]J. Crank, G. S. Park, Diffusion in polymers, London: Academic, 1968

[49]R. M. Barrer, Some Properties of Diffusion Coefficients in Polymers, J. Phys. Chem., 1957, 61(2), 178–189

[50]J. C. Slater, Introduction to chemical physics. New York: McGraw Hill, 1939

[51] J. S. Vrentas, J. L. Duda, Diffusion in Polymer-Solvent Systems. 11. A Predictive Theory

for the Dependence of Diffusion Coefficienta on Temperature, Concentration, and Molecular Weight. J. Polym. Sci.: Poly. Phys. Ed. 197713, 15, 417-439.

[52]C. A. Kumins, T. K. Kwei, Diffusion in polymer. New York: Academic, 1968

[53] A. T. DiBenedetto, D. R. Paul, An interpretation of gaseous diffusion through polymers using fluctuation theory, J Polym. Sci., 1964, 2, 1001-1015

[54] H. L. Frisch, D. Klempner, Penetrant diffusion in polymers, Macromolecules 1971 4 237-238

[55] Barrer, R. M.; Barrie, J. A.; Slatter, J. Sorption and Diffusion in Ethyl Cellulose. Part I. History Dependence of Sorption Isotherms and Permeation Rates. J. Polym. Sci. 1957a, 23, 315-329

[56] J. S. Vrentas, J. L. Duda, H. F. Mark, N. M. Bikales, C. G. Overberger, G. Menges, Encyclopedia of polymer science and engineering, vol. 5. New York: Wiley, 1986, 36-68

[57]K. Ganesh R. Nagrajan J. L. Duda, Rate of gas transport in glassy polymers: a free volume based predictive model, Ind. Eng. Chem. Res. 1992, 31, 746-755

[58] Cohen, M. H.; Turnbull, D. Molecular Transport in Liquids and Glasses. J. Chem. Phys. 1959,31, 1164-1169.

[59]D. w. van Krevelen, Properties of polymers, Amsterdam: Elsevier, 1990, 72-76

[60]S. A. Stern, Polymers for gas separations: the next decade, J Membr Sci, 1994, 94, 1-7

[61]Y. Ichiraku, S.A. Stern, An investigation of the high gas permeability of poly (1-Trimethylsilyl-1-Propyne), J Membr Sci, 1987, 34, 5–18

[62]D.R. Paul, O.M. Ebra-Lima, Pressure-induced diffusion of organic liquids through highly swollen polymer membranes, J. Appl. Polym. Sci., 1970, 14, 2201-2208

[63]R.T. Jacobsen, R.B. Stewart, A.F. Myers, An equation of state for oxygen and nitrogen, Adv. Cryog. Eng., 1972, 18, 248-256

[64]T. Nakagawa, H.B. Hopfenberg, V. Stannett, Transport of fixed gases in radiation-stabilized poly(vinyl chloride), J. Appl. Polym. Sci., 1971, 15, 231-235

[65] W. J. Koros, R. T. Chern, R. W. Rousseau, Handbook of separation process technology, New York, Wiley, 1987

[66] T. Masuda, E. Isobe, T. Higashimura, K. Takada, Poly [1-(trimethylsilyl)-1-propyne]: A new high polymer synthesized with transition-metal catalysts and characterized by extremely high gas permeability, J. Amer. Chem. Soc., 1983, 105, 7473-7480

[67] H. Masuda, Y. Nakata, K. Takada, Application of the substituted poly (acetylene) to a semi-permeable membrane, Polym. Prepr. (Japan), 1983, 32, 2925-2931

[68] T. Masuda, E. Isobe, T. Higashimura, Polymerization of 1-(trimethylsilyl)-2-propyne by halides of niobium (V) tantalum(V) polymer properties, Macromolecules, 1985, 18, 841-856

[69] K. Takada, H. Matsuya, T. Masuda, T. Higashimura Gas permeability of polyacetylenes carrying substituents, J. Appl. Polym. Sci., 1985, 30, 1605-1609

[70]C.E. Rogers, Solubility and diffusivity, in: D. Fox, M.M. Labes, A. Weissberger (Eds.), Physical Chemistry of the Organic Solid State, Interscience Publishers, New York, NY, 1965

[71]S.A. Stern, Gas permeation processes, in: R.E. Lacey, S. Loeb (Eds.), Industrial Processing with Membranes, Wiley-Interscience, New York, NY, 1972

[72]S.A. Stern, H.L. Frisch, The selective permeation of gases through polymers, Ann. Rev. Mater. Sci., 1981, 11, 523-528

[73]H.L. Frisch, S.A. Stern, Diffusion of small molecules in polymers, Critical Rev. Solid State and Mater. Sci., CRC Press, Boca Raton, FL, 1983

[74]J. Crank, The Mathematics of Diffusion (2nd edition.), The Clarendon Press, Oxford, 1975

[75] K. Kamide, S. Manabe, Material science of synthetic membranes, ACS symposium series 269, Washington, DC, American Chemical Society, 1985

[76]V.M. Shah, B.J. Hardy, S.A. Stern, Solubility of carbon dioxide, methane, and propane in silicone polymers. Effect of polymer side chains, J. Polym. Sci., 1986, 24, 2033-2039

[77]N.E. Van Huff, G. Houghton, J. Coull, Equation of state and compressibilities for gaseous carbon dioxide in the range 0° to 600°C, and 0 to 150 atm, J. Chem. Eng. Data, 1963, 8, 336-342

[78]M. Benedict, G.B. Webb, L.C. Rubin, An empirical equation for thermodynamic properties of light hydrocarbons their mixtures, Chem. Eng. Prog., 1951, 47 (1951), 419-427

[79] T. R. Cuthbert, N. J. Wagner, M. E. Paulaitis, Molecular dynamics simulation of penetrant diffusion in amorphous polypropylene: diffusion mechanisms and simulation size effects, Macromolecules, 1999, 32, 5017-5028

[80]V. Ullal, D. E. Spearot , Molecular Simulation (2013): Molecular dynamics simulation of O_2 diffusion in polydimethylsiloxane (PDMS) and end-linked PDMS networks, Molecular Simulation, DOI: 10.1080/08927022.2013.830183

[81] H. Fujita, J. Crank, G. S. Park, Diffusion in polymers, New York, Academic, 1968, 75-105

[82] M. Kujawski, L. Rakesh, K. Gala, A. Jensen, B. Fahlman, Z. R. Feng, D. K. Mohanty, Molecular dynamics simulation of polyamidoamine dendrimer-fullerene conjugates:

generations zero through four. J. Nanosci. Nanotechnol. 2007, 7(4-5), 1670-1673.

[83] V. Kalra, S. Mendez, F. Escobedo, Y. L. Joo, Coarse-grained molecular dynamics simulation on the placement of nanoparticles within symmetric di-block copolymers under shear flow. J. Chem. Phys. 2008, 128(16), 164909-164919.

[84] M. A. Mazo, L. I. Manevitch, E. B. Gusarova, M. Y. Shamaev, A. A. Berlin, N. K. Balabaev, G. C. Rutledge, Molecular Dynamics Simulation of Thermomechanical Properties of Montmorillonite Crystal. 1. Isolated Clay Nanoplate. J. Phys. Chem. B 2008, 112(10), 2964-2969.

[85] B. J. Alder, T. E. Wainwright. Studies in Molecular Dynamics. I. General Method, J. Chem. Phys. 31 (2), (1959) 459-463.

[86] A. Rahman, Correlations in the Motion of Atoms in Liquid Argon, Phys Rev 136 (2), 1964, 405-411

[87] J. P. Mesirov, K. Schulten, D. W. Sumners, Mathematical Applications to Biomolecular Structure and Dynamics, IMA Volumes in Mathematics and Its Applications, 82. New York: Springer-Verlag, 1996, 218–247

[88] P. S. de Laplace, Oeuveres Completes de Laplace, Theorie Analytique des Probabilites, Paris, France, Gauthier-Villars, 1820

[89] W. Smith, T. R. Forester, I. T. Todorov, The DLPOLY user manual. STFC Daresbury

Laboratory, Cheshire, UK, 2010

[90] F. Mueller-Plathe, Calculation of the free energy for gas absorption in amorphous polypropylene. Macromolecules, 1991, 24, 6475-6480.

[91] T. R. Cuthbert, N. J. Wagner, M. E. Paulaitis, Molecular simulation of glassy polystyrene: size effects on gas solubilities. Macromolecules, 1997, 30, 3058-3062.

[92] N. F. A. Van der Vegt, W. J. Briels, M. Wessling, H. Strathmann, Free energy calculations of small molecules in dense amorphous polymers: effect of the initial guess configuration in molecular dynamics studies. J. Chem. Phys. 1996, 105, 8849-8857.

[93] N. F. A. van der Vegt, W. J. Briels, M. Wessling, H. Strathmann, The sorption induced glass transition in amorphous glassy polymers. J. Chem. Phys. 1999, 110, 11061-11069.

[94] N. F. A. van der Vegt, W. J. Briels, Efficient sampling of solvent free energies in polymers. J. Chem. Phys. 1998, 109, 7578-7582.

[95] T. R. Cuthbert, N. J. Wagner, M. E. Paulaitis, Molecular dynamics simulation of penetrant diffusion in amorphous polypropylene: diffusion mechanisms and simulation size effects. Macromolecules 1999, 32, 5017-5028.

[96] P. V. Pant, R. H. Boyd, Molecular dynamics simulation of diffusion of small penetrants in polymers. Macromolecules, 1993, 26, 679−686.

[97] S. J. Weiner, P. A. Kollman, D. A. Case, U. C. Singh, C. Ghio, G. Alagona, S. Profeta, P. Weiner, A new force field for molecular mechanical simulation of nucleic acids and proteins. J. Am. Chem. Soc, 1984, 106, 765-784.

[98] W. L. Jorgensen, J. Tirado-Rives, The OPLS force field for proteins. energy minimizations for crystals of cyclic peptides and crambin. J. Am. Chem. Soc. 1988, 110, 1657–1666.

[99] R. M. Sok, H. J. C. Berendsen, W. F. van Gunsteren, Molecular dynamics simulation of the transport of small molecules across a polymer membrane. J. Chem. Phys. 1992, 96, 4699-4704.

[100] N. F. A. van der Vegt, Temperature dependence of gas transport in polymer melts: molecular dynamics simulations of CO_2 in polyethylene. Macromolecules, 2000, 33, 3153-3160.

[101] F. Muller-Plathe, Calculation of the free energy for gas absorption in amorphous polypropylene. Macromolecules, 1991, 24, 6475-6479.

[102] A. Vedani, D. W. Huhta, A new force field for modeling metalloproteins. J. Am. Chem. Soc. 1990, 112, 4159-4161.

[103] Y. Yampolskii, I. Pinnau, B. D. Freeman, Materials science of membranes for gas and vapor separation. John Wiley & Sons Ltd, West Sussex, England, 2006

[104] B. Widom, Some topics in the theory of fluids. J. Chem. Phys. 1963, 39, 2808-2813.

[105] B. R. Svenssona, C. E. Woodwarda, Widom's method for uniform and non-uniform electrolyte solutions, Molec. Phys. 1988, 64, 247-259.

[106] J. Vrabec, M. Kettler, H. Hasse, Chemical potential of quadrupolar two-centre Lennard-Jones fluids by gradual insertion. Chem. Phys. Lett., 2002, 356, 431-436.

[107] J. Crank, G. S. Park, Diffusion in polymers. Academic Press, London, New York, 1968

[108] A. L. Laskar, Diffusion in materials. Kluwer Academic Publishers, Boston, 1990

[109] B. D. Freeman, I. Pinnau, Gas and liquid separations using membranes: an overview (In advanced materials for membrane separations). ACS Symposium Series, American Chemical Society, Washington, DC, 2004

[110] S. Sourirajan, Reverse Osmosis, Academic Press, New York, 1970

[111] C. D Wick, L. X. Dang, Molecular mechanism of transporting a polarizable iodide anion across the water-CCl4 liquid/liquid interface J. Chem. Phys. 2007, 126, 134702

[112] H. Yasuda, A. Petterlin, Diffusive and bulk flow transport in membranes, J. Appl. Polym. Sci., 1973, 17, 433-439

[113] A. Petterlin, A. Yasuda, Comments on the relationship between hydraulic permeability

and diffusion in homogeneous swollen membranes, J. Polym. Sci., Polym. Phys. Ed., 1974, 13, 1215-1223

[114] D. Rose, I. Benjamin, Free Energy of Transfer of Hydrated Ion Clusters from Water to an Immiscible Organic Solvent J. Phys. Chem. B 2009, 113, 9296– 9303

[115] A. Gupta, A. Chauhan, D. I. Kopelevich, Molecular modeling of surfactant covered oil-water interfaces: Dynamics, microstructure, and barrier for mass transport J. Chem. Phys. 2008, 128, 234709

[116] D.R. Paul, O.M. Ebra-Lima, Pressure-induced diffusion of organic liquids through highly swollen polymer membranes, J. Appl. Polym. Sci., 1970, 14, 2201-2206

[117]D.R. Paul, Diffusive transport in swollen polymer membranes, H.B. Hopfenberg (Ed.), Permeability of Plastic Films and Coatings, Pergamon, New York, 1974

[118]D.R. Paul, Further comment on the relation between hydraulic permeation and diffusion J. Polym. Sci., 1974, 12, 1221-1227

[119]D.R. Paul, J.D. Paciotti, O.M. Ebra-Lima, Hydraulic permeation of liquids through swollen polymeric networks: II Liquid mixtures, J. Appl. Polym. Sci., 1975, 19, 1837-1841

[120]D.R. Paul, J.D. Paciotti, Driving force for hydraulic and pervaporation transport in homogeneous membranes, J. Polym. Sci., Polym. Phys. Ed., 1975, 13, 1201-1207

[121]D.R. Paul, The solution diffusion model for swollen membranes, Sep. Purif. Methods, 1976, 5, 33-39

[122] H.K. Lonsdale, U. Merten, R.L. Riley, Transport properties of cellulose acetate osmotic membranes, J. Appl. Polym. Sci., 1965, 9, 1344-1350

[123]U. Merten, Transport properties of osmotic membranes in Desalination by Reverse Osmosis MIT Press, Cambridge, MA, 1966

[124] S. Rosenbaum, O. Cotton, Steady-state distribution of water in cellulose acetate membrane, J. Polym. Sci., 1969, 7, 101-106

[125]S.N. Kim, K. Kammermeyer, Actual concentration profiles in membrane permeation Sep. Sci., 1970, 5, 679-683

[126]A. Mauro, Some properties of ionic and non ionic semipermeable membranes Circulation, 1960, 21, 845-851

[127] F. Theeuwes, R.M. Gale, R.W. Baker, Transference, a comprehensive parameter governing permeation of solutes through membranes, J. Membrane Sci., 1976, 1 (1976), 3-7

[128] F.W. Greenlaw, W.D. Prince, R.A. Shelden, E.V. Thompson, The effect of diffusive permeation rates by upstream and downstream pressures, J. Membrane Sci., 1977, 2, 141-

[129] J.G. Wijmans, R.W. Baker, A simple predictive treatment of the permeation processes in pervaporation, J. Membrane Sci., 1993, 79, 101-107

[130] T. Okeda, T. Matsuura, Theoretical and experimental study of pervaporation on the basis of pore flow mechanism, R. Bakish (Ed.), Proc. Sixth Int. Conf. Pervaporation Chem. Ind., Ottawa, Canada, Bakish Materials, Corp, P.O. Box 148, Engelwood, NJ, 1992

[131] C. D. Wick, L. X. Dang, Recent advances in understanding transfer ions across aqueous interfaces Chem. Phy. Lett. 2008, 458, 1– 5

[132] Y. N. Ahn, A. Gupta, A. Chauhan, D. Kopelevich, I.Molecular Transport through Surfactant-Covered Oil–Water Interfaces: Role of Physical Properties of Solutes and Surfactants in Creating Energy Barriers for Transport Langmuir 2011, 27 (6) 2420– 2436

[133] B. C. Garrett, G. K. Schenter, A. Morita, Molecular Simulations of the Transport of Molecules across the Liquid/Vapor Interface of Water Chem. Rev. 2006, 106, 1355– 1374

[134] K. Zhurov, E. J. F. Dickinson, R. G.. Compton, Dynamics of Ion Transfer Potentials at Liquid–Liquid Interfaces J. Phys. Chem. B 2011, 115, 6909– 6921

[135] K. Zhurov, E. J. F. Dickinson, R. G.. Compton, Dynamics of ion transfer potentials at liquid–liquid interfaces: the case of multiple species, J. Phys. Chem. B 2011, 115, 12429–12440

[136] T. V. Lee, Oxidation adjacent to oxygen of alcohols by activated DMSO methods, Comp. Org. Synth. 1991, 7, 291

[137] P. Katalin, D. Mária, H. George, Properties of the liquid-vapor interface of water-dimethyl sulfoxide mixtures. a molecular dynamics simulation and ITIM analysis study, J. Phys. Chem. C 2010, 114, 12207– 12220

[138] B. Hess, GROMACS 4: Algorithms for highly efficient, load-balanced, and scalable molecular simulation, J. Chem. Theory Comput. 2008, 4, 435– 447

[139] Y. J. Zheng, R. L. Ornstein, A molecular dynamics and quantum mechanics analysis of the effect of dmso on enzyme structure and dynamics, J. Am. Chem. Soc. 1996, 118, 4175–4180

[140] W. G. Hoover, Canonical dynamics: Equilibrium phase-space distributions, Phys. Rev. A, 1985, 31, 1695– 1697

[141] M. Parrinello., A. Rahman., Polymorphic transitions in single crystals: A new molecular dynamics method, J. Appl. Phys. 1981, 52, 7182

[142] T. Darden, D. York, L. Pedersen, Particle mesh Ewald: an N.log(N) method for Ewald sums in large systems, J. Chem. Phys. 1993, 98, 10089– 10092

[143] U. Essmann, L. Perera, M. L. Berkowitz, T. Darden, H. Lee, L. G. Pedersen, A smooth

particle mesh Ewald method, J. Chem. Phys. 1995, 103, 8577– 8593

[144] B. Hess, H. Bekker, H. J. C. Berendsen, LINCS: a linear constraint solver for molecular simulations J. Comput. Chem. 1997, 18, 1463– 1472

[145] D. A. McQuarrie, Statistical Mechanics; Harper & Row: New York, 1976

[146]B. Buesser, A. J. Grohn, and S. E. Pratsinis, Sintering Rate and Mechanism of TiO2 Nanoparticles by Molecular Dynamics, J. Phys. Chem. C 2011, 115, 11030–11035

[147]P. M. Oliver, G. W. Watson, E. Toby Kelsey and S. C. Parker, Atomistic simulation of the surface structure of the TiO2 polymorphs rutile and anatase, J. Mater. Chem., 1997, 7(3), 563–568

[148]H. le Roux, L. Glasser, Transferable potentials for the Ti–O system, J. Mater. Chem., 1997, 7(5), 843–851

[149] V. Swamy, J. D. Gale, Transferable variable-charge interatomic potential for atomistic simulation of titanium oxides, Phys. Rev. B, 62(9), 2000, 5407-5412

[150] M. Matsui and M. Akoagi, Molecular dynamics simulation of the structural and physical properties of the four polymorphs of TiO2, Mol. Simul., 1991, 6, 239-247

[151] M. Alimohammadi, K. A. Fichthorn, A force field for the Interaction of water with TiO_2 surfaces, J. Phys. Chem. C ,2011, 115, 24206–24214

[152]Q. Yang, L. E. Achenie, M. A. Cai, Comparing penetrants transport and mechanical property of composite poly (4-methyl-2-pentyne) and two forms of silica nanoparticles through molecular dynamics simulation, Ind. Eng. Chem. Res, 2013, 52 (19), 6462–6469

[153]Q. Yang, L. E. Achenie, Molecular dynamics simulation of penetrants transport in composite poly (4-methyl-2-pentyne) and silica nanoparticles. J. Phys. Chem. C, 2012, 116, 7409-7415

Appendix

```
// The code is to create structure
//


#include "stdafx.h"
#include "math.h"
#include "fstream.h"
#include "iostream.h"
#include <ctime>
#include <cstdlib>


#define N 150
#define M 125
#define S 585
#define length 63 //121  //strip length
#define PI 3.14159265
#define rcut 9.0
#define Rgas 1.987e-3 //??kcal/mol/k
#define T 500.01
//#define F 1.54  //bond length
#define Distance 1.80

double F=1.526;
//double cx=54.94, cy=54.94, cz=54.94;  //30.4
#define centerDist  12.5//2.5


//double cx=54.94, cy=54.94, cz=54.94;  //30.4
//double cx=30.508, cy=29.147, cz=29.147;
double cx=30.508, cy=30.508, cz=30.508;

struct CModPoint{
public:
        int nStrip;
        int indx;
        double x;
        double y;
        double z;

//      CPoint(){
```

```
//                  new CPoint;
//          }
};

struct CPoint{
public:
        double x;
        double y;
        double z;

//      CPoint(){
//                  new CPoint;
//          }
};

int ifchange(double x, double y, double z);
CModPoint gModPoints[200];
CPoint gPoints[N];
CPoint gSPoints[S][N], gSPoints1[S][N], gHP[S][N][3];
int gN=0;
int gnMod=0;
int gS=0;

//int gS=0;
int nLimit=5;
double dmin=9.;

int change(double& x, double &y, double&z);

double calculateDist(CPoint p1, CPoint p2){
        double d=pow(p1.x-p2.x,2)+pow(p1.y-p2.y,2)+pow(p1.z-p2.z,2);
        return sqrt(d);
};
//vdw
double calculateU(double r){
        double u=2.739e5*exp(-3.329*r)-2.942e3/pow(r,6);
        return u;
}

double calculateV(double phi);

double phi[M];
//possib list
double createPhiPL(double p[M]){
        p[0]=0;
        double vList[M], ptotal=0.;
        for(int i=1; i<=20; i++){
                phi[i]=(i)*9./180.*PI;
                vList[i]=calculateV(phi[i]);
                p[i]=exp(-vList[i]/Rgas/T);
                ptotal+=p[i];
```

```
	}

	for(i=1;i<=20;i++)
		p[i]/=ptotal;
	for(i=2;i<=20;i++)
		p[i]+=p[i-1];
	return 0.;
}



//inversion di-hedron
double calculateV(double phi){
	double v=0.5*4.1*(0.163*(1-cos(phi))+(1-0.163)*(1-cos(3*phi)));
	return v;
}

int leng[N];

double calculateE(CPoint pnew){
	double e=0, e1=0.;
	CPoint pnew1;
	pnew1.x=pnew.x;
	pnew1.y=pnew.y;
	pnew1.z=pnew.z;
	int ifchanged=change(pnew1.x, pnew1.y, pnew1.z);
	if(ifchanged==1)
	{
/*		gnMod++;
		if(gN==length)
			gModPoints[gnMod].nStrip=gS;
		else
			gModPoints[gnMod].nStrip=gS;
		gModPoints[gnMod].indx=gN;
		gModPoints[gnMod].x=pnew1.x;
		gModPoints[gnMod].y=pnew1.y;
		gModPoints[gnMod].z=pnew1.z;


		gSPoints1[gS][gN-1].x=newp[indx].x;
		gSPoints1[gS][gN].y=newp[indx].y;
		gSPoints1[gS][gN].z=newp[indx].z;  */


		for(int j=1;j<=gS-1;j++){
			if(leng[j]==length+3){
			for(int k=4;k<=leng[j];k++){
				double d=calculateDist(gSPoints1[j][k], pnew1);
				if(d<dmin)
					dmin=d;
```

```
                                        if(d<rcut)
                                                e1+=calculateU(d);
                                }
                                }
                        }
                        for(int i=4;i<=gN;i++){
                                double r=calculateDist(gSPoints1[gS][i], pnew1);
//                              if(r<dmin) dmin=r;
                                if(r<rcut)
                                        e1+=calculateU(r);
                        }
                }

                for(int j=1;j<=gS-1;j++){
                        if(leng[j]==length+3){
                        for(int k=4;k<=leng[j];k++){
                                double d=calculateDist(gSPoints[j][k], pnew);
                                if(d<dmin) dmin=d;
                                if(d<rcut)
                                        e+=calculateU(d);
                        }
                        }
                }
                for(int i=4;i<=gN;i++){
                        double r=calculateDist(gPoints[i], pnew);
//                      if(r<dmin) dmin=r;
                        if(r<rcut)
                                e+=calculateU(r);
                }
                if(ifchanged==1&&e1>e) return e1;
                return e;
}


void createNewPoint(CPoint p01, CPoint p02, CPoint p03){


        double xx1= rand();
//      double yy2=RAND_MAX;
        double yy1= xx1/RAND_MAX;

        CPoint p1, p2;
        p1.x=p03.x-p02.x;
        p1.y=p03.y-p02.y;
        p1.z=p03.z-p02.z;

        p2.x=p02.x-p01.x;
        p2.y=p02.y-p01.y;
        p2.z=p02.z-p01.z;
```

```
	double a=112./180.*PI;

	if((gN-gN/2*2)==0){
		F=1.600;
		a=109.5/180.*PI;
	}
	else{
		F=1.600;
		a=144./180.*PI;
	}


	double A1=(cos(a)/F*p2.y-cos(beta)/F*p1.y)/(p1.x*p2.y-p2.x*p1.y);
	double B1=-(p1.z*p2.y-p2.z*p1.y)/(p1.x*p2.y-p2.x*p1.y);
	double A2=(cos(a)/F*p2.x-cos(beta)/F*p1.x)/(p1.y*p2.x-p2.y*p1.x);
	double B2=-(p1.z*p2.x-p2.z*p1.x)/(p1.y*p2.x-p2.y*p1.x);
	double A=1+B1*B1+B2*B2;
	double B=2*(A1*B1+A2*B2);
	double C=A1*A1+A2*A2-1;
	if(yy1>0.5)
		p.z=(-B+sqrt(B*B-4*A*C))/2/A;
	else
		p.z=(-B-sqrt(B*B-4*A*C))/2/A;

	p.x=A1+B1*p.z;
	p.y=A2+B2*p.z;
	p.z*=F;
	p.x*=F;
	p.y*=F;
		p.z+=p03.z;
		p.x+=p03.x;
		p.y+=p03.y;



}


int SelectPhi(double pL[M]){


	if(gN<3)
		return 3;
//aa:	srand(time(0));
//	for(int kk=1; kk<=20; kk++){

	int indx, indx1;
	double phi0[M], emin, emin1;
	CPoint newp[M], newp1[N];
	for(int j=1; j<=15; j++){
/*		double xx1= rand();
```

```
//                double yy2=RAND_MAX;
                  double rad= xx1/RAND_MAX;
                  for(int i=0; i<=19; i++){
                        if(rad>=pL[i]&&rad<pL[i+1])
                              phi0[j]=phi[i]+(rad-pL[i])*PI;
                  }
bb:               createNewPoint(gPoints[gN-2], gPoints[gN-1], gPoints[gN], newp[j], phi0[j]);
//*/

bb:               double xx1= rand();
//                double yy2=RAND_MAX;
                  double rad= xx1/RAND_MAX;
                  for(int i=0; i<=19; i++){
                        if(rad>=pL[i]&&rad<pL[i+1])
                              phi0[j]=phi[i]+(rad-pL[i])*PI;
                  }
                  createNewPoint(gPoints[gN-2], gPoints[gN-1], gPoints[gN], newp[j], phi0[j]);


                              CPoint pCenter;
                              pCenter.x=0.;
                              pCenter.y=0.;
                              pCenter.z=0.;

                              CPoint pp;
                              for(int mm1=-nLimit;mm1<=nLimit;mm1++){
                                    pp.x=newp[j].x+mm1*cx;
                                    for(int mm2=-nLimit;mm2<=nLimit;mm2++){
                                          pp.y=newp[j].y+mm2*cy;
                                          for(int mm3=-nLimit;mm3<=nLimit;mm3++){
                                                pp.z=newp[j].z+mm3*cz;


                  if(calculateDist(pp,pCenter)<centerDist){
                        goto bb;
//                            double d=calculateDist(pp, p2);
//                            if(d<dd)
//                                  dd=d;
                                          }//mm3
                                    }//mm2
                              }//mm1


                  }
/*                int ifc=0;
/*                int ifc=0;
                  if(ifc=ifchange(newp[j].x, newp[j].y, newp[j].z)==1){
                        for (int k=1;k<=20;k++){
                              createNewPoint(gPoints[gN-2], gPoints[gN-1], gPoints[gN],
newp1[k], phi[k]);
                              double e1=calculateE(newp1[k]);
```

```
                        if(k==1){
                                emin1=e1;
                                indx1=1;}
                        else{
                                if(e1<emin1){
                                        emin1=e1;
                                        indx1=k;
                                }
                        }
                }
        } */


//              createNewPoint(gPoints;
                double e=calculateE(newp[j]);
                if(dmin<Distance) {
                        dmin=9.0;
                        return 0;
                        double xx2= rand();
//                      double yy2=RAND_MAX;
                        double rad2= xx2/RAND_MAX;
                        if(rad2<0.333)
                                phi0[j]=0;
                        if(rad2>=0.333&&rad2<0.666)
                                phi0[j]=PI/2.;
                        if(rad2>=0.666)
                                phi0[j]=PI;
//                      goto bb;
                }
/*              if(ifc==1&&e>emin1){
                        e=emin1;
                        newp[j].x=newp1[indx1].x;
                        newp[j].y=newp1[indx1].y;
                        newp[j].z=newp1[indx1].z;
                }  */

                if(j==1) {
                        emin=e;
                        indx=1;
                }
                else{
                        if(e<emin){
                                emin=e;
                                indx=j;
                        }
                }
        }


        gN+=1;
        gPoints[gN].x=newp[indx].x;
```

```
		gPoints[gN].y=newp[indx].y;
		gPoints[gN].z=newp[indx].z;
		gSPoints[gS][gN].x=newp[indx].x;
		gSPoints[gS][gN].y=newp[indx].y;
		gSPoints[gS][gN].z=newp[indx].z;



		gSPoints1[gS][gN].x=newp[indx].x;
		gSPoints1[gS][gN].y=newp[indx].y;
		gSPoints1[gS][gN].z=newp[indx].z;
		if(int changed=change(gSPoints1[gS][gN].x, gSPoints1[gS][gN].y,
gSPoints1[gS][gN].z)==1)
		{
			gnMod++;
			if(gN==length)
				gModPoints[gnMod].nStrip=gS;
			else
				gModPoints[gnMod].nStrip=gS;
			gModPoints[gnMod].indx=gN;
			gModPoints[gnMod].x=newp[indx].x;//gSPoints1[gS][gN].x;
			gModPoints[gnMod].y=newp[indx].y;//gSPoints1[gS][gN].y;
			gModPoints[gnMod].z=newp[indx].z;//gSPoints1[gS][gN].z;
		}
		return 1;
//		if(gN==length){
//			gS++;
//			gN=3;
//		}
}

//		}


void createFirst3(int nStrips){
//	srand(time(0));
		for(int i=1; i<=nStrips; i++){
//			srand(time(0));
cc:			double xx1=rand();
			double xx2=rand();
			double xx3=rand();
			double xx4=rand();
			double rad1=xx1/RAND_MAX;
			double rad2=xx2/RAND_MAX;
			double rad3=xx3/RAND_MAX;
			double rad4=xx4/RAND_MAX;
			double xt=cx*(rad1-0.5);
			double yt=cy*(rad2-0.5);
			double zt=cz*(rad3-0.5);

			double xt1, yt1, zt1;
```

```
//              if(rad4<0.333){

                if(rad4<0.5){
                gSPoints[i][1].x=xt;
                gSPoints[i][1].y=yt;
                gSPoints[i][1].z=zt;


                        xt1=xt+0.209;
                        yt1=yt+0.8535;
                        zt1=zt+1.265;
//              }
/*              if(rad4>=0.333&&rad4<0.666){
                        xt1=xt+0.209;
                        zt1=zt+0.8535;
                        yt1=yt+1.265;
                }
                if(rad4>=0.666){
                        zt1=zt+0.209;
                        yt1=yt+0.8535;
                        xt1=xt+1.265;
                }  */


                gSPoints[i][2].x=xt1;
                gSPoints[i][2].y=yt1;
                gSPoints[i][2].z=zt1;

//              if(rad4<0.333){

                gSPoints[i][3].x=xt1+0.209;
                gSPoints[i][3].y=yt1-0.8535;
                gSPoints[i][3].z=zt1+1.265;
                } //if
                else{
                gSPoints[i][3].x=xt;
                gSPoints[i][3].y=yt;
                gSPoints[i][3].z=zt;


                        xt1=xt+0.209;
                        yt1=yt+0.8535;
                        zt1=zt+1.265;
//              }
/*              if(rad4>=0.333&&rad4<0.666){
                        xt1=xt+0.209;
                        zt1=zt+0.8535;
                        yt1=yt+1.265;
                }
                if(rad4>=0.666){
                        zt1=zt+0.209;
```

```
                    yt1=yt+0.8535;
                    xt1=xt+1.265;
                }  */




                gSPoints[i][2].x=xt1;
                gSPoints[i][2].y=yt1;
                gSPoints[i][2].z=zt1;

//              if(rad4<0.333){

                gSPoints[i][1].x=xt1+0.209;
                gSPoints[i][1].y=yt1-0.8535;
                gSPoints[i][1].z=zt1+1.265;
                }  //else



                        CPoint pCenter;
pCenter.x=0.;
pCenter.y=0.;
pCenter.z=0.;



        if(calculateDist(gSPoints[i][1],pCenter)<centerDist||calculateDist(gSPoints[i][2],pCent
er)<centerDist||calculateDist(gSPoints[i][3],pCenter)<centerDist){
                    goto cc;
                }


//              }

/*              if(rad4>=0.333&&rad4<0.666){

                gSPoints[i][3].x=xt1+0.209;
                gSPoints[i][3].z=zt1-0.8535;
                gSPoints[i][3].y=yt1+1.265;

                }
                if(rad4>=0.666){

                gSPoints[i][3].z=zt1+0.209;
                gSPoints[i][3].y=yt1-0.8535;
                gSPoints[i][3].x=xt1+1.265;

                }  */
```

```
//                gSPoints[i][3].x=xt1+0.209;
//                gSPoints[i][3].y=yt1-0.8535;
//                gSPoints[i][3].z=zt1+1.265;

                gSPoints1[i][1].x=gSPoints[i][1].x;
                gSPoints1[i][1].y=gSPoints[i][1].y;
                gSPoints1[i][1].z=gSPoints[i][1].z;
                gSPoints1[i][2].x=gSPoints[i][2].x;
                gSPoints1[i][2].y=gSPoints[i][2].y;
                gSPoints1[i][2].z=gSPoints[i][2].z;
                gSPoints1[i][3].x=gSPoints[i][3].x;
                gSPoints1[i][3].y=gSPoints[i][3].y;
                gSPoints1[i][3].z=gSPoints[i][3].z;


        } //for


}

int ifchange(double x, double y, double z){
//notice
        return 0;
                bool ifchanged=false;
        if(fabs(x)>cx/2.){
                ifchanged=true;
                if(x>0)
                        x=x-abs(x/cx+0.5)*cx;
                else
                        x=x+abs(x/cx-0.5)*cx;
        }
        if(fabs(y)>cy/2.){
                ifchanged=true;
                if(y>0)
                        y=y-abs(y/cy+0.5)*cy;
                else
                        y=y+abs(y/cy-0.5)*cy;
        }
        if(fabs(z)>cz/2.){
                ifchanged=true;
                if(z>0)
                        z=z-abs(z/cz+0.5)*cz;
                else
                        z=z+abs(z/cz-0.5)*cz;
        }
        if(ifchanged==false)
                return 0;
        else
                return 1;
}
```

```
int change(double& x, double &y, double&z){
	return 0;//notice
	bool ifchanged=false;
	if(fabs(x)>cx/2.){
		ifchanged=true;
		if(x>0)
			x=x-abs(x/cx+0.5)*cx;
		else
			x=x+abs(x/cx-0.5)*cx;
	}
	if(fabs(y)>cy/2.){
		ifchanged=true;
		if(y>0)
			y=y-abs(y/cy+0.5)*cy;
		else
			y=y+abs(y/cy-0.5)*cy;
	}
	if(fabs(z)>cz/2.){
		ifchanged=true;
		if(z>0)
			z=z-abs(z/cz+0.5)*cz;
		else
			z=z+abs(z/cz-0.5)*cz;
	}
	if(ifchanged==false)
		return 0;
	else
		return 1;
}



int main(int argc, char* argv[])
{
  srand(time(0));
	ofstream outfile, outfile1;
//	double h=R/M, maxE=0;
	outfile.open("resultdata.txt");
	outfile1.open("resultdata1.txt");

	gN=3;
	double pL[M];
	createPhiPL(pL);

//	createFirst3(S);
	int nfull=0;

	int ncount=0;
	for(int j=1; j<=S; j++){
		gS=j;
```

```
                gN=3;
                createFirst3(S);
                gPoints[3].z=gSPoints[j][3].z, gPoints[3].y=gSPoints[j][3].y,
gPoints[3].x=gSPoints[j][3].x;
                gPoints[1].z=gSPoints[j][1].z, gPoints[1].y=gSPoints[j][1].y,
gPoints[1].x=gSPoints[j][1].x;
                gPoints[2].z=gSPoints[j][2].z, gPoints[2].y=gSPoints[j][2].y,
gPoints[2].x=gSPoints[j][2].x;

//              gPoints[3].z=0.5608, gPoints[3].y=0.7592, gPoints[3].x=3.7524;
//              gPoints[1].z=0.1869, gPoints[1].y=0.8157, gPoints[1].x=1.25080;
//              gPoints[2].z=0.3738, gPoints[2].y=-0.0565, gPoints[2].x=2.5016;

//              gPoints[3].z=gSPoints[j][3].z, gPoints[3].y=gSPoints[j][3].y,
gPoints[3].x=gSPoints[j][3].x;
//              gPoints[1].z=gSPoints[j][1].z, gPoints[1].y=gSPoints[j][1].y,
gPoints[1].x=gSPoints[j][1].x;
//              gPoints[2].z=gSPoints[j][2].z, gPoints[2].y=gSPoints[j][2].y,
gPoints[2].x=gSPoints[j][2].x;

//              for(int k=1; k<=30; k++){

//                      SelectPhi(pL);
//                              k--;
//              gN++;
//              }
                int k=1;
                while(gN<length+3&&k<500){
                        SelectPhi(pL);
                        k++;
                }
//      gN--;
                leng[j]=gN;
                if(gN==length+3)
                        nfull++;



                double vx=0, vy=0, vz=0;


                if(leng[j]==length+3){

                for(int i=4; i<=leng[j]; i++){

///   To add hydrogen atom into the chains              double xx1= rand();
//              double yy2=RAND_MAX;
//              double rad= xx1/RAND_MAX;
///   To add hydrogen atom into the chains
                        double a1=-(gSPoints1[j][i].x-gSPoints[j][i-1].x);
                        double b1=-(gSPoints1[j][i].y-gSPoints[j][i-1].y);
```

```
//        double kk=1.096;  //for C-H
          double kk=1.880;  //for C-Si
//                b1=1.e-6;

          double c1=-(gSPoints1[j][i].z-gSPoints[j][i-1].z);
          double d1=calculateDist(gSPoints1[j][i], gSPoints[j][i-1]);
          double zz1=rand();
          double detx=zz1/RAND_MAX/2.;
          double A=cos(109.5/180.*3.14159265)*d1-a1*detx;

          double detz1, detz2, dety1, dety2;
        if(fabs(b1)>1.e-2){
          double alpha=1.+c1*c1/b1/b1;
          double beta=-2*A*c1/b1/b1;
          double zeta=A*A/b1/b1+detx*detx-1.;
          double sq=beta*beta-4*alpha*zeta;
          if(sq<0){
                sq=-sq;
                zz1=rand();
                goto nn;
          }

          detz1=(-beta+sqrt(sq))/2./alpha;
          detz2=(-beta-sqrt(sq))/2./alpha;

          dety1=(A-c1*detz1)/b1;
          dety2=(A-c1*detz2)/b1;}

        else{
nn:             detz1=A/c1;
                detz2=A/c1;
                double sq=1.-detx*detx-detz1*detz1;
                if(sq<0){
                        detz1=0.1;
                        detz2=0.1;
                }
                dety1=sqrt(1.-detx*detx-detz1*detz1);
                dety2=-sqrt(1.-detx*detx-detz1*detz1);
        }

          double x=gSPoints[j][i].x+detx*kk;
          double y1=gSPoints[j][i].y+dety1*kk;
          double y2=gSPoints[j][i].y+dety2*kk;
          double z1=gSPoints[j][i].z+detz1*kk;
          double z2=gSPoints[j][i].z+detz2*kk;

          gHP[j][i][1].x=x;
          gHP[j][i][2].x=x;
          gHP[j][i][1].y=y1;
          gHP[j][i][2].y=y2;
```

```
                    gHP[j][i][1].z=z1;
                    gHP[j][i][2].z=z2;



///   To add hydrogen atom into the chains
///   To add hydrogen atom into the chains

                    ncount++;
//                  change(gPoints[i].x, gPoints[i].y, gPoints[i].z);
//                  change(gSPoints[j][i].x, gSPoints[j][i].y, gSPoints[j][i].z);
//                          outfile<<"C                         "<<i+(gS-1)*length-
3<<endl;
                    if((i-i/2*2)==0){
                        if(i==4||i==66)
                            outfile<<"CP                        ";
                        else
                            outfile<<"OP                        ";
                            outfile<<ncount<<endl;//<<"     ,    "<<j<<endl;
                            outfile<<"
"<<gSPoints1[j][i].x<<","<<gSPoints1[j][i].y<<","<<gSPoints1[j][i].z<<endl;
                            outfile<<"      "<<vx<<","<<vy<<","<<vz<<endl;
                    }
                    else{
                            outfile<<"SiP
"<<ncount<<endl;//<<"     ,    "<<j<<endl;
                            outfile<<"
"<<gSPoints1[j][i].x<<","<<gSPoints1[j][i].y<<","<<gSPoints1[j][i].z<<endl;
                            outfile<<"      "<<vx<<","<<vy<<","<<vz<<endl;

//  Output hydrogen atoms_____________________________________________
                            outfile<<"CP
"<<ncount<<endl;//<<"     ,    "<<j<<endl;
                            outfile<<"
"<<gHP[j][i][1].x<<","<<gHP[j][i][1].y<<","<<gHP[j][i][1].z<<endl;
                            outfile<<"      "<<vx<<","<<vy<<","<<vz<<endl;

                            outfile<<"CP
"<<ncount<<endl;//<<"     ,    "<<j<<endl;
                            outfile<<"
"<<gHP[j][i][2].x<<","<<gHP[j][i][2].y<<","<<gHP[j][i][2].z<<endl;
                            outfile<<"      "<<vx<<","<<vy<<","<<vz<<endl;
                    }


//  Output hydrogen atoms_____________________________________________

                }
                }
```

```
            if(nfull==5)  //strip #
            break;

        }//for j
/*                          if(k-k/2*2==1){
                                outfile1<<"C"<<endl;
                                outfile1<<"        "<<x2<<","<<y2<<","<<z2<<endl;
                                outfile1<<"        "<<vx<<", "<<vy<<","<<vz<<endl;
                            } */


        double dd=10;
        CPoint p2;
        int mpoint=0;

        do{
            double xx1=rand();
            double xx2=rand();
            double xx3=rand();
            double xx4=rand();
            double rad1=xx1/RAND_MAX;
            double rad2=xx2/RAND_MAX;
            double rad3=xx3/RAND_MAX;
            double rad4=xx4/RAND_MAX;
            double xt=cx*(rad1-0.5);
            double yt=cy*(rad2-0.5);
            double zt=cz*(rad3-0.5);
            p2.x=xt;
            p2.y=yt;
            p2.z=zt;


        for(int j=1;j<=gS; j++){
            if (leng[j]==33){
                for (int k=4;k<=length+3;k++){
                    double d=calculateDist(gSPoints1[j][k], p2);
                    if(d<dd)
                        dd=d;
                }
            }
        }

        if(dd>2){
            mpoint++;
            outfile<<"MMM        "<<p2.x<<","<<p2.y<<","<<p2.z<<endl;
            dd=10.;
        }
        dd=10;
        }
        while(mpoint<13);
```

```
	CPoint pt[N];
	pt[1].x=5.;

	for(int i=1;i<=gnMod;i++){

//                                      outfile<<"M
"<<gModPoints[i].nStrip<<"                      "<<gModPoints[i].indx<<endl;
//                                      outfile<<"
"<<gModPoints[i].x<<","<<gModPoints[i].y<<","<<gModPoints[i].z<<endl;
//                                      outfile<<"        "<<vx<<","<<vy<<","<<vz<<endl;
	}




	outfile.close();
	outfile1.close();



	return 0;
}
```